On the non-uniqueness of friction forces and the systematic computation of dynamic response boundaries for turbine bladed disks with contacts

On the Non-Uniqueness of Friction Forces and the Systematic Computation of Dynamic Response Boundaries for Turbine Bladed Disks with Contacts

Erhan Ferhatoglu†[1], Stefano Zucca†

† Department of Mechanical and Aerospace Engineering, Politecnico di Torino, Corso Duca degli Abruzzi 24, 10129 Torino, Italy

ABSTRACT

Turbine bladed disks with friction contacts may have a large scattering of dynamic response amplitudes in laboratory conditions even for two consecutive tests. The non-repeatability of experimental studies might directly be related to a physical phenomenon associated with an uncertainty in contact forces. This observation has also been computationally shown in many studies with non-unique contact forces and multiple responses obtained for the same set of inputs. This study presents a numerical aspect and a deeper insight for understanding the variability observed in the periodic vibration analysis of turbine bladed disks with friction damping. A novel method based on an optimization algorithm is proposed to systematically detect the nonlinear dynamic response boundaries. The main idea of the developed approach is to minimize the system loss factor which ultimately determines the damping ability of the structure. In the meanwhile, algebraic set of dynamic balance equations are simultaneously imposed as the nonlinear constraints to be satisfied. In this way, two cases with the minimum values of the positive and negative loss factor determine the upper and the lower boundaries, respectively. The method is validated and demonstrated on a realistic turbine bladed disk with friction interfaces on the shrouds and on the blade-disk interface. Several case studies are performed on different cases by using the state of the art 2D friction model with varying normal load. The results show that the limits of the variability range can be successfully captured by utilizing the offered optimization algorithm. The great contribution of the study is also discussed with some accompanying numerical drawbacks.

Keywords: Nonlinear Forced Response, Friction Damping, Non-Unique Contact Forces, Multiple Solutions, Optimization Algorithm, Turbine Bladed Disks.

[1] Corresponding Author
E-mail addresses: erhan.ferhatoglu@polito.it (Erhan Ferhatoglu), stefano.zucca@polito.it (Stefano Zucca)

1. INTRODUCTION

Remarkable developments have been performed in the field of undesired vibration reduction with friction damping for turbo-machinery applications over the last four decades. Since detuning of the natural frequencies has been generally unsuccessful to avoid large stresses due to high modal density of the rotors and wide spectrum of the excitation force; starting from the first studies proposed in 1980s [1-3], intentional implementation of the dry friction into large turbine structures has greatly facilitated to deal with high cycle fatigue problems resulted by high vibration amplitudes [4]. Engineers in academia and industry have developed several design solutions to be able to mitigate large oscillatory loads. Some examples are under-platform dampers (UPD) [5, 6], ring dampers [7, 8], mid-span dampers [9, 10] or the use of contacts in the shrouds [11, 12] and in the blade-disk interfaces [13, 14].

Great success of the friction damping over the years has promoted the researchers to delve into further in experimental studies as well as the computational ones. However, interpretation of the test results in laboratory conditions have always become challenging due to difficulties for large assemblies with sub-components and loss of repeatability in the measurements. There are several sources for the ineffectiveness of the real life application tests. Some of them may be related to wearing in the contact surfaces, misalignments in the assemblies, manufacturing errors, residual stresses and etc. Brake et. al deeply investigated the prospective problems for response variability in experimental studies, where the interested readers may refer to their paper [15]. One of the most important reasons for the variability in the response, which is elaborately studied in this paper, comes from the uncertainty of the friction forces. According to the Coulomb's friction law, tangential contact force value for a fully stuck contact should always stay within a range whose boundaries are determined by limit values obtained with a multiplication of the surface friction coefficient and the normal force on that surface. This fact generates non-unique tangential forces within a range, where all of the possibilities are true. In addition to this fully stuck interface; if there is at least one another slipping contact in the system, multiple steady state response for totally same system parameters is possible due to interaction between normal and tangential directions. It is worth here highlighting that the definition of *uncertainty* in the literature is slightly ambiguous. It is used as a very general term to explain different phenomena [15]; for instance, uncertainty of friction parameters, uncertainties due to wearing in contact surfaces, uncertainty in the measurements and etc. In this study, uncertainty mainly refers to non-uniqueness of tangential

friction forces. Correspondingly, the dynamic response variability is investigated in the context of above described fact.

The uncertainty phenomenon was analytically shown as the first time by Yang et. al [16, 17] on wedge dampers. The authors reported that non-unique steady-state vibration amplitudes exist due to uncertainty of the contact forces even if all the input parameters are kept same. Detailed investigation is then performed on UPDs by Zucca et. al [18] stating different static balance of the damper leads a range of variability in the turbine dynamics. Although this phenomenon has been shown in several applications in the last decades [16-20], the researchers presented all the nonlinear response curves in their computational studies, probably unconsciously, as if they are unique. However, recent experimental investigations performed exactly on the same conditions for UPDs [21-23] showed that different initial state of the damper in successive tests give rise to a huge variability in vibration amplitudes and resonance frequencies. The authors of [23] declared that the large scattering of the variability cannot only be explained by micro changes in the contact surface (e.g. microwear) since it generally induces a slow changing progress in the response behavior. All of these experimental observations prove that the variability obtained in computational studies is not a modeling artifact but a real physical phenomenon. The latest numerical researches on different systems also point out the same fact [10, 24, 25].

Non-unique vibration amplitudes creates a range in frequency response graphs, whose upper and lower boundaries take the highest attention in terms of engineering point of view, because the turbine components are generally designed with respect to the largest vibration amplitudes. For this purpose, Yang et. al [16, 17] offered an analytical technique for wedge dampers to estimate the highest oscillatory amplitudes. The authors utilized geometric relations in contact state configurations for the computation of extreme friction forces, where the detailed information can be found in [26]. Similarly, Ferhatoglu et. al [25] very recently developed a numerical approach for the response boundaries of wedge dampers modeled with macro-slip contact elements. It is shown that the all possible solutions can be bounded by the frequency response curves obtained by utilizing the limit tangential force values. However, these two approaches are not suitable for the systems undergoing micro-slip behavior. On the other hand, besides finding the limits methodically, one can also search for it manually by assigning a set of static displacements as an initial guess. This idea with some filtering algorithm is used in [23]. Despite the simplicity of this approach, its feasibility is quite limited due to high computational burden. In addition, the selected initial set may not become

sufficient to be able to capture all potential contact states, which can result to miss correct response boundaries. Zucca et. al [20] also proposed a way to compute always the identical steady-state response within the variability range.

There are also various studies in the literature, which use statistical and stochastic approaches to be able to predict the response bounds in frictional systems [27-29]. However, these studies are not directly relevant to the uncertainty and the variability terms used in the concept of this work. It should be noted that the state of the art in the literature for variability studies and for the frequency response limits has not reached its maturity level yet.

Each abovementioned techniques have advantageous aspects but limited capabilities for a systematic computation of dynamic response boundaries in the context of non-unique friction force uncertainty. In line with this purpose, in this paper, a novel numerical method based on an optimization algorithm is proposed for the determination of periodic response boundaries of the variability range. Unlike the other studies in the literature, developed method is a deterministic and a generalized approach which makes it suitable for all type of turbine bladed disk applications having friction damping with a large number of contacts. The method particularly uses the system's damping loss factor as the objective function to minimize through an optimization procedure as well as it concurrently satisfies the nonlinear set of algebraic equations obtained with Harmonic Balance Method (HBM). With this novel side of the method, the upper and the lower boundaries are systematically computed regardless of the system's complexity degree. The method is demonstrated on a realistic large turbine bladed disk having the contact on the blade tip with shrouds and in the root with blade-disk interfaces. Validation of the proposed approach is firstly performed on shroud contacts by comparing the obtained results with those computed with the reference technique [25]. The boundaries are then calculated and shown by performing several case studies on the shrouds and on the blade-disk interfaces. All of the analyses showed that the method is considerably adequate to be able to detect the nonlinear response boundaries. To the best of authors' knowledge, this study offers the first deterministic and systematic technique in turbo-machinery applications for the computation of nonlinear response limits in the context of variability phenomenon due to non-uniqueness of friction force.

2. METHODOLOGY

2.1 Dynamics of Turbine Bladed Disks with Contact Interfaces

Turbine bladed disks are large structures having complex three-dimensional shapes with possibly several sub-components as representatively shown in Fig. 1a. It consists of n_s totally identical sectors divided evenly over a 2π angle under the assumption of absence of mistuning effects, i.e. variations of the system properties for each sector. This enables to utilize cyclic symmetry by applying proper boundary conditions on the sector interfaces [30]. In this way, full bladed disk model can be reduced to only fundamental sector which is an isolated one subjected to excitation and contact forces as representatively shown in Fig. 1b. This approach greatly facilitates to deal with large models with high computational burden. In this study, the blade is assumed tuned and all of the theoretical derivations are presented for the fundamental sector.

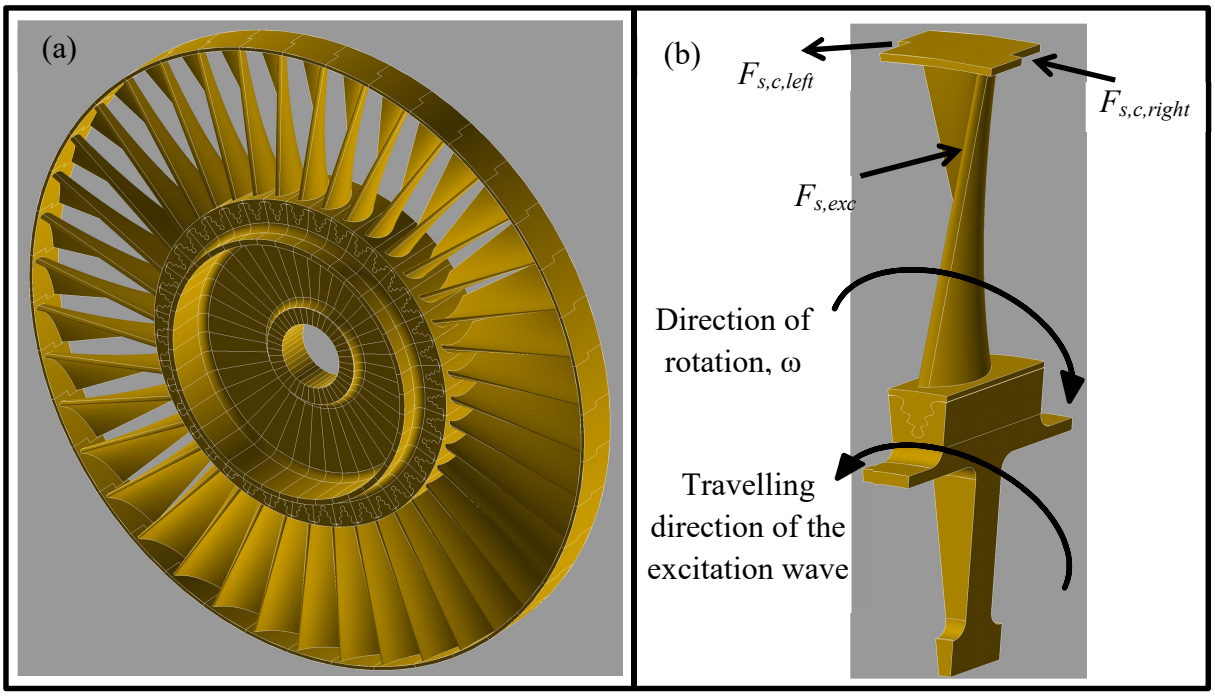

Fig. 1 (a) Turbine Bladed Disk, (b) Fundamental Sector

The nonlinear dynamics of the fundamental sector excited by a periodic external force is governed by the second order differential equation in time domain as

$$\mathbf{M}_s\ddot{\mathbf{q}}_s(t)+\mathbf{C}_s\dot{\mathbf{q}}_s(t)+\mathbf{K}_s\mathbf{q}_s(t)+\mathbf{F}_{s,c}(t)-\mathbf{F}_{s,exc}(t)=\mathbf{0}\,. \tag{1}$$

Here, $\mathbf{M}_s$, $\mathbf{C}_s$ and $\mathbf{K}_s$ denote the symmetric and positive definite sector matrices of mass, viscous damping and stiffness, respectively. $\mathbf{q}_s(t)$ represents the generalized coordinates vector of the fundamental sector. $\mathbf{F}_{s,c}(t)$ and $\mathbf{F}_{s,exc}(t)$ are the nonlinear contact force and periodic excitation force vectors, respectively. It should be noted that contact forces are directly dependent to system response. Gyroscopic effects due to Coriolis forces is also neglected in Eq. (1).

The turbine bladed disks are subjected to periodic travelling excitation as the rotor hub rotates with an angular velocity, ω. This implies a time delay between adjacent sectors with δt = T/ n_s, being T is the period of the excitation (T = 2π/ω). Since the excitation is periodic, it can be decomposed to its harmonic components as

$$\mathbf{F}_{s,exc}(t) = \hat{\mathbf{F}}^0_{s,exc} + \mathrm{Im}\left(\sum_{h=1}^{H} \hat{\mathbf{F}}^h_{s,exc} e^{ih\omega t} \right). \tag{2}$$

$\hat{\mathbf{F}}^0_{s,exc}$ and $\hat{\mathbf{F}}^h_{s,exc}$ are the real and complex amplitude vectors of the 0$^{\text{th}}$ and h^{th} harmonics, respectively. H is the truncated harmonic number and i is the unit imaginary number.

The main interest in the dynamics of the turbine bladed disks is generally the steady-state vibration amplitudes which can be assumed periodic, as well. Therefore, steady state response and correspondingly the contact forces can also be written with their harmonic components as

$$\mathbf{q}_s(t) = \hat{\mathbf{q}}^0_s + \mathrm{Im}\left(\sum_{h=1}^{H} \hat{\mathbf{q}}^h_s e^{ih\omega t} \right) \quad \text{and} \quad \mathbf{F}_{s,c}(t) = \hat{\mathbf{F}}^0_{s,c} + \mathrm{Im}\left(\sum_{h=1}^{H} \hat{\mathbf{F}}^h_{s,c} e^{ih\omega t} \right), \tag{3}$$

respectively. Similarly, $\hat{\mathbf{q}}^0_s$ and $\hat{\mathbf{F}}^0_{s,c}$ are the real bias, $\hat{\mathbf{q}}^h_s$ and $\hat{\mathbf{F}}^h_{s,c}$ are the complex amplitude vectors of the h^{th} harmonics.

In accordance with the Fourier-Galerkin method, substitution of Eqs. (2) and (3) into Eq. (1) yield to obtain nonlinear algebraic set of equations in frequency domain as

$$\begin{aligned} \mathbf{K}_s \hat{\mathbf{q}}^0_s + \hat{\mathbf{F}}^0_{s,c} - \hat{\mathbf{F}}^0_{s,exc} &= \mathbf{0} \\ \left(-(h\omega)^2 \mathbf{M}_s + ih\omega \mathbf{C}_s + \mathbf{K}_s \right) \hat{\mathbf{q}}^h_s + \hat{\mathbf{F}}^h_{s,c} - \hat{\mathbf{F}}^h_{s,exc} &= \mathbf{0} \quad (h = 1, \cdots, H) \end{aligned}, \tag{4}$$

where all the nonlinear equations are coupled to each other via contact forces, $\hat{\mathbf{F}}^0_{s,c}$ and $\hat{\mathbf{F}}^h_{s,c}$.

In turbo-machinery field, contact interfaces on the bladed disks are widely modeled with contacts elements. In this study, two dimensional contact element with variable normal load, also the so-called as Jenkins element, is utilized. Due to its simplicity and effectiveness, it has been widely used in many studies [10, 18-20, 23]. The contact element is able to capture the macro-slip contact behavior in two in-plane tangential directions and the normal motion in out-of-plane direction. Three springs perpendicular to each other in each direction are utilized to represent the contact stiffness, i.e. $k_{t,1}$, $k_{t,2}$ and k_n. Two sliders are used in tangential directions to pair the contact points. It should be noted that two sliding directions are decoupled in the contact element, as representatively shown in Fig. 2a.

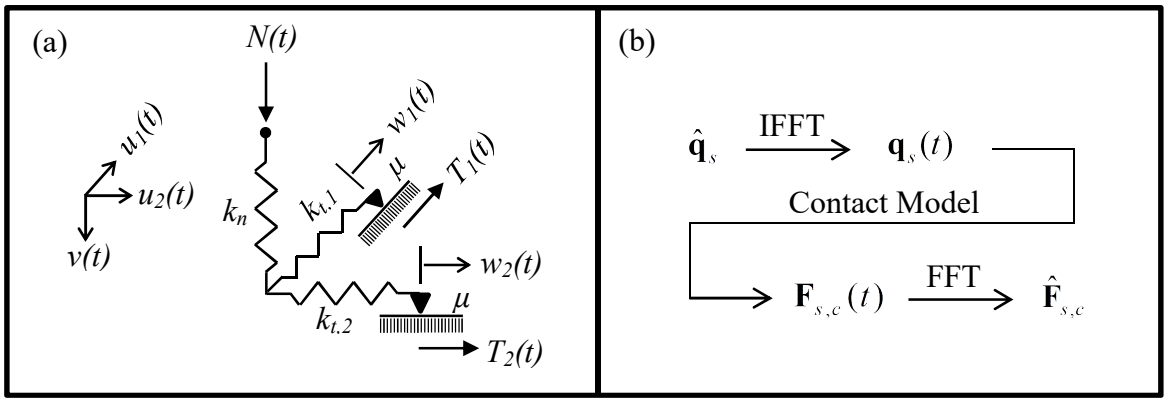

Fig. 2 (a) Two Dimensional Contact Element with Variable Normal Load, (b) Alternating Frequency/Time Method

Normal Force, $N(t)$, and Tangential Forces in two decoupled directions, $T_{1,2}(t)$, can be calculated in Jenkins model at time instant t as

$$N(t) = \max\left(k_n v(t), 0\right) \qquad \text{and} \qquad T_{1,2}(t) = \begin{cases} k_{t_{1,2}}\left[u_{1,2}(t) - w_{1,2}(t)\right] & \text{stick state} \\ \mu N(t)\,\text{sign}\left(\dot{w}_{1,2}(t)\right) & \text{slip state} \\ 0 & \text{lift-off state} \end{cases}, \tag{5}$$

where $v(t)$, $u(t)$ and $w(t)$ represent the relative displacement in normal direction, relative displacement in tangential direction and the slip motion of the slider, respectively. μ is the friction coefficient of the contact surface. It should be noted the slider position of the element is an unknown parameter at time t, which prevents to calculate the tangential force value directly. In order to overcome this problem, a very simple predictor-corrector technique [12] can be utilized to compute tangential forces. In this technique, it is first assumed that the contact element has a stick state at time instant t and the position of the slider is arbitrarily estimated by guessing an initial value. The assumption is then checked according to the

Coulomb's law. If the assumption is valid, initial guess becomes correct; if not, it means that the contact element is under either alternating stick-slip or lift-off state. In this case, the computation of the tangential force does not require the information of the slider position as can be seen in Eq. (5). Interested readers may refer to [12] for a more detailed investigation. Moreover, in order to compute contact forces in frequency domain, $\hat{\mathbf{F}}_{s,c}$, Alternating Frequency/Time (AFT) algorithm [31] is used. In this approach, time domain nonlinear responses, $\mathbf{q}_s(t)$, are first obtained by performing Inverse Fast Fourier Transform (IFFT) to Fourier coefficients, $\hat{\mathbf{q}}_s$. Nonlinear contact forces, $\mathbf{F}_{s,c}(t)$, are then calculated by using Eq (5). Lastly, the forces computed in time domain are transformed back to frequency domain by applying Fast Fourier Transform (FFT) to obtain complex amplitudes, $\hat{\mathbf{F}}_{s,c}$.The procedure is also summarized schematically in Fig. 2b. The simplicity of the approach makes it quite feasible to utilize in the nonlinear analysis instead of taking the numerical integration of Fourier coefficients.

2.2 Non-Unique Contact Forces and Multiple Responses

Computation of tangential contact force in stick state, as explained in the previous section, creates a set of correct values within a range. In other words, the uncertainty of the slider position makes the tangential force non-unique. In order to understand this phenomenon further, consider a fully stuck element whose contact force graph and hysteresis curve are representatively shown in Fig. 3. According to the Coulomb's law, tangential force, *T(t),* should always be confined into a range, whose boundaries are determined by $\mu N(t)$ and $-\mu N(t)$, for a full stick cycle. It should be noted that although the dynamic part of the tangential force is the same, the static component, T^0, is non-unique and can vary within the range between T^0_{min} and T^0_{max}. As a consequence, an infinite number of configurations is possible, each corresponding to a given value of T^0 such that $T^0_{min} \leq T^0 \leq T^0_{max}$. It is worth noting that non-unique contact forces exist when the element is fully stuck. If the contact element undergoes an alternating stick-slip or an alternating stick-slip-separation motion, the periodic contact forces are uniquely defined, as representatively shown in Fig. 4.

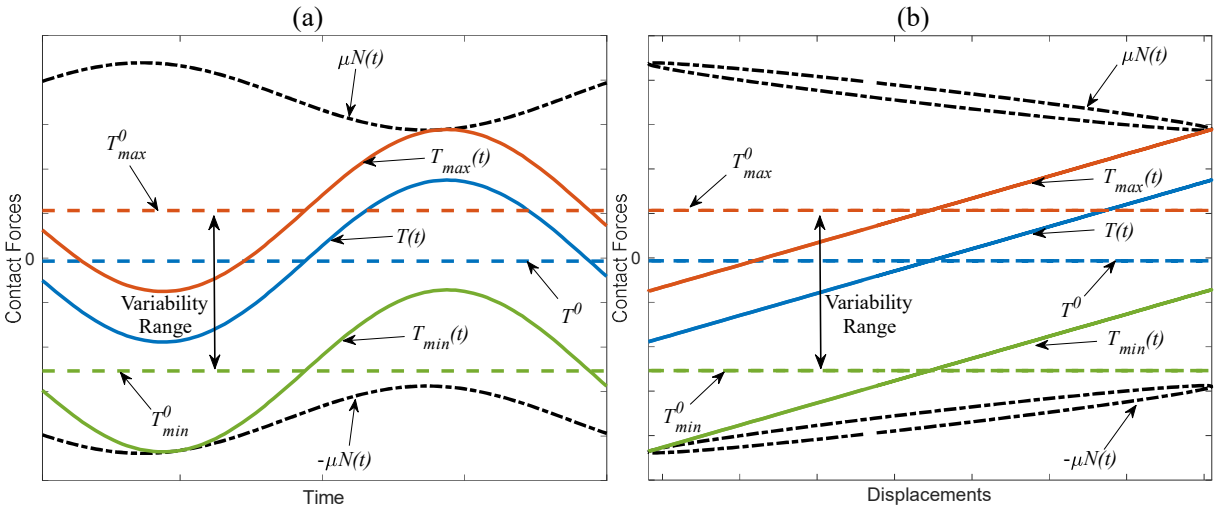

Fig. 3 (a) Time Histories of Contact Forces, (b) Hysteresis Curves for a Full Stick Cycle [25]

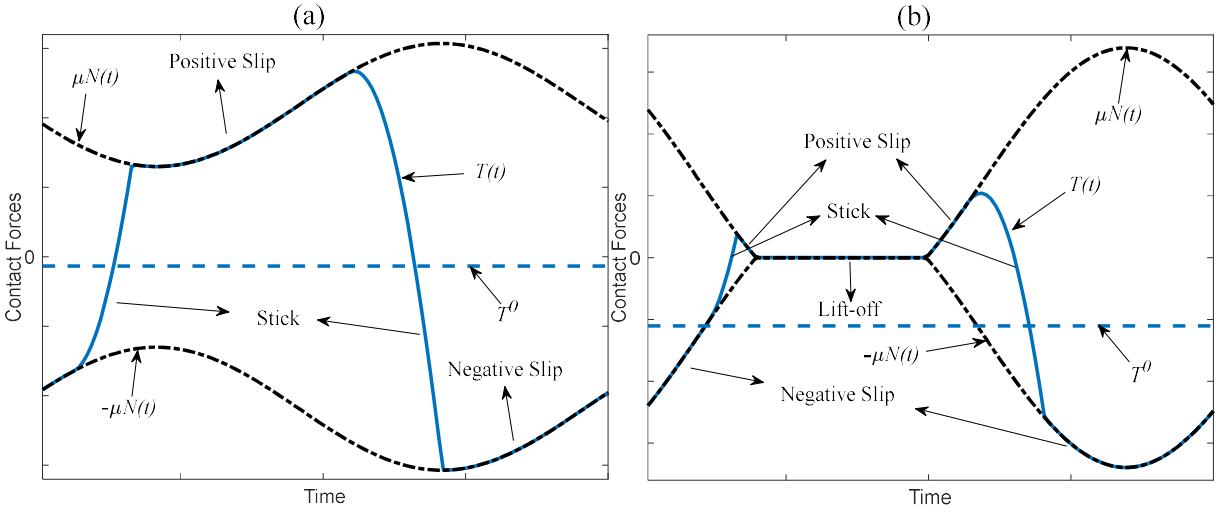

Fig. 4 (a) Time Histories of Contact Forces for an Alternating Stick-Slip Cycle, (b) Time Histories of Contact Forces for an Alternating Stick-Slip-Separation Cycle [25]

In order to understand the effects of non-unique contact forces on the system response, first consider a Jenkins element which is under a harmonic motion of $\mathrm{q}(t)$. Contact force, $\mathrm{f}_c(t)$, in steady-state can be generically written as a multiplication of contact element's equivalent stiffness, k_{eq}, and equivalent damping, c_{eq}, terms with the input motion as

$$\mathrm{f}_c(t) = \left(\mathrm{k}_{eq}(\hat{q}) + i\mathrm{c}_{eq}(\hat{q})\right) \times \mathrm{q}(t), \tag{6}$$

where $\hat{q}$ denotes the response amplitude of the input motion. k_{eq} and c_{eq} correspond to real and imaginary parts of complex describing functions that are introduced for the harmonic vibration analysis of nonlinear structures in [32]. They are the physical representation of the equivalent stiffness and damping of the contact element for a certain harmonic input motion

$q(t)$. Their equations for a one-dimensional Jenkins element with a constant normal load N^0 and under a harmonic input motion, i.e. $q(t) = \hat{q}\cos(\omega t)$, is given in Appendix.

For the illustration of the multiple responses, now consider a body with contact interfaces, modeled by means of multiple Jenkins elements, as the one shown in Fig. 5. In this system, consider a steady-state dynamic configuration, in which elements A and C are in a fully stuck cycle, while the other ones (B and D) are undergoing an alternating stick-slip motion. The static tangential components $T^0{}_{\mathrm{A}}$ and $T^0{}_{\mathrm{C}}$ are non-unique. This means that the static normal components of the slipping contact elements ($N^0{}_{\mathrm{B}}$ and $N^0{}_{\mathrm{D}}$) can also be non-unique due to the static equilibrium of the body. As a result, the equivalent stiffness and damping at contacts B and D may change with different values of $N^0{}_{\mathrm{B}}$ and $N^0{}_{\mathrm{D}}$ (see Appendix). This leads to multiple contact force vectors $\hat{\mathbf{F}}^0_{s,c}$ and $\hat{\mathbf{F}}^h_{s,c}$ in Eq. (4) and to multiple response levels for the same physical system under the identical excitation frequency and forces.

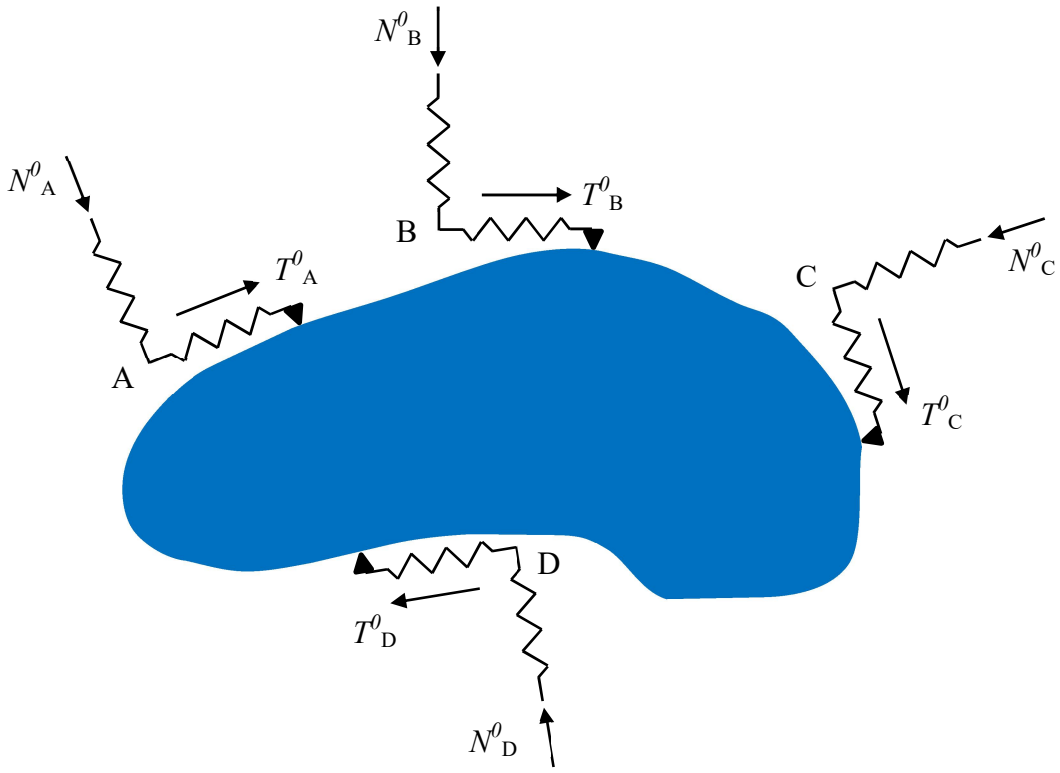

Fig. 5 A Body with Multiple Contact Elements

It is important to note that multiple responses only exist in case of partial slip. If all the contact elements (A-D) are in a full stick cycle, k_{eq} and c_{eq} do not differ and the solution ends up a unique linear response. Similarly, if the contact undergoes a gross-slip motion (i.e. all elements enter the slip and/or the separation state during the periodic motion), only one

single solution occurs since the variability comes from the fully stuck elements. Interested readers can refer to [25] for a more detailed investigation of the geometric coupling and the variability phenomenon.

Multiple solutions can be easily obtained by following different strategies. Some examples are to change frequency sweep direction [23], frequency step [10], or initial guess of the static displacements in the nonlinear analyses [23]. One another straightforward approach is also to change initial guess of the tangential contact force before starting the computation of friction forces, as it was proposed in [25]. In this approach, the initial value of the tangential force at the very beginning of the predictor-corrector strategy, described in the previous section, is set to an arbitrary value so that the Coulomb's law is satisfied. In a more general way, the tangential force value with a stick state assumption can be initially guessed at $t = t_{ini}$ for each contact element in the system as

$$T(t_{ini}) = m \times \mu N(t_{ini}) , \tag{7}$$

where m is a multiplier coefficient and may be different for each contact element. It should also be noted that m can theoretically take a value in a range between –1 and 1, i.e. $-1 \le m \le 1$. After the predictor-corrector algorithm, if the contact element fully sticks at the end of the cycle, one of the multiple tangential forces in the variability range (see Fig. 3) is computed. In this way, the non-unique contact forces can be obtained by simply changing the value of m in different analyses. Therefore, if there is a partial-slip motion in the contacts, the multiple solution of the response becomes possible with non-unique contact forces.

2.3 Periodic Response Boundaries with an Optimization Algorithm

Multiple alternatives of possible steady-state solutions bring much more complexity to interpretation of the results. Especially, if there is a strong geometric cross-coupling between tangential and normal directions on different contact surfaces in the system, such as in wedge or mid-span dampers, the variability range can be unpredictably large. For example, Ferhatoglu et. al [10] computationally showed in the mid-span dampers that there may be even ten times difference between two possible response amplitudes at the same frequency. In addition, Gastaldi et. al [23] observed 50 Hz resonance shift in UPDs after two consecutive tests in laboratory conditions. All of these computational and experimental studies prove that variability phenomenon may create huge effects and cannot be ignored in the design of frictional systems. From the engineering point of view, the boundaries always take the core

attention and need to be determined. In this study, an optimization algorithm aiming to minimize the loss factor of the system is developed to detect the highest and the lowest limits in steady-state vibration amplitudes.

First, consider the work done by an external periodic force for the fundamental sector per one vibration cycle as

$$W = \int_0^{2\pi/\omega} \dot{\mathbf{q}}_s^{\mathrm{T}}(t)\,\mathbf{F}_{s,exc}(t)\,dt\,. \tag{8}$$

For a vibrating system under a steady-state condition, the main energy input to system due to periodic excitation is equivalent to the work done, and it is balanced by the sum of dissipated energy, ΔW_{dis}, and maximum potential energy, U_{pot}, for the corresponding response amplitude level as

$$W = \Delta W_{dis} + U_{pot}\,. \tag{9}$$

Eq. (9) is valid for a vibration-in-unison pattern, which means all of the system points reach their maximum oscillation amplitudes and pass through zero simultaneously. Therefore, the kinetic energy at time instant *t,* when the dynamic response reaches to amplitude, can be considered zero and all of the mechanical energy for this case becomes equal to maximum potential energy. Reduction of the vibration response in frictional systems is associated with the dissipated energy. However, in turbine bladed disks, the amount of dissipated energy is not an absolute indicator for a meaningful interpretation of damping present in the system. In order to quantify damping, loss factor, η, defined as the proportion of the total energy dissipated over one cycle to the maximum potential energy corresponding to the vibration amplitude[33, 34] is used, and it is shown as

$$\eta = \frac{\Delta W_{dis}}{2\pi U_{pot}} = \frac{\Delta W_{visc} + \Delta W_{fric}}{2\pi\left(U_{blad} + U_{cont}\right)}, \tag{10}$$

where ΔW_{visc}, ΔW_{fric}, U_{blad} and U_{cont} represent the dissipated energy by viscous material damping, dissipated energy by friction damping, potential energy of the linear bladed disk without any contact and potential energy due to contacts, respectively.

Dissipated energy by viscous damping and potential energy for one sector of the bladed disk are directly related to linear matrices of the system and they can be calculated for one vibration period as [33],

$$\Delta W_{visc} = \pi \times \omega \times \hat{\mathbf{q}}_s^{\mathrm{H}} \mathbf{C}_s \hat{\mathbf{q}}_s , \tag{11}$$

$$U_{blad} = \frac{1}{4} \hat{\mathbf{q}}_s^{\mathrm{H}} \mathbf{K}_s \hat{\mathbf{q}}_s , \tag{12}$$

where superscript H represents the hermitian operator.

ΔW_{fric} and U_{cont} are the energy terms introduced by the contact. It should be noted that friction element has a complex contact force value, where the real part is associated with stiffness and imaginary part is related to damping as shown in Eq. (6). Hence, dissipated energy by friction damping and the potential energy due to contacts for one vibration period can also be computed as [33]

$$\Delta W_{fric} = \pi \times \mathrm{Im}\left(\hat{\mathbf{q}}_s^{\mathrm{H}} \hat{\mathbf{F}}_{s,c} \right), \tag{13}$$

$$U_{cont} = \frac{1}{4} \mathrm{Re}\left(\hat{\mathbf{q}}_s^{\mathrm{H}} \hat{\mathbf{F}}_{s,c} \right), \tag{14}$$

respectively. It has been shown in many studies that the loss factor, η, is the absolute parameter for quantifying the total damping in the system. Its numerical value in free or fully stuck linear cases, in which the only contribution is made by viscous damping, is expected considerably small since no dissipation is supplied by friction. When the slip takes place in contact interface, it starts increasing and may reach to its local maximum. Then, it can decrease to its minimum values. Detailed investigation of the behavior of loss factor with respect to changing several parameters can be found in [33, 34]. In this study, a novel approach utilizing an optimization algorithm with the minimization of the loss factor is developed for the computation of the non-unique response boundaries.

In the proposed approach, in addition to the unknown response vector, $\hat{\mathbf{q}}_s$, in Eq. (4), another variable unknown vector of multiplier coefficients, $\mathbf{m}$, in which the number of array terms is twice of the number of contact elements (N_c), is firstly defined as

$$\mathbf{m} = \left[m_1, m_2, \cdots, m_{N_c}, \cdots, m_{2N_c} \right]^{\mathrm{T}}. \tag{15}$$

These multipliers do not directly appear in the nonlinear set of algebraic Eq. (4) as an unknown, but they can be considered as the so-called internal unknowns of the contact element. In particular, the i^{th} term of the vector, m_i, represents the ratio between the tangential force and the Coulomb limit force at the very beginning ($t = t_{ini}$) of the predictor-corrector loop used to determine the periodic contact forces in time domain (see *Section 2.2*), as

$$T_i(t_{ini}) = m_i \times \mu N_i(t_{ini}) \qquad \left(i = 1, 2, \cdots, 2N_c\right), \tag{16}$$

with $-1 \le m_i \le 1$. It should be noted that the number of the multipliers is the double of the number of contact elements, because one 2D Jenkins element consists two uncoupled sliders for two tangential directions (see Fig. 2a). If 1D Jenkins element had been used in the system, the number of the multipliers would have become equal to the number of contact elements, since one 1D Jenkins element has only a single slider in the tangential direction.

When the number of 2D contact elements in the system is only one, two different multipliers (m_1 and m_2), which are the unknowns corresponding to two uncoupled in-plane tangential directions, need to be multiplied with the Coulomb limit force, separately. In this case, the response boundaries of the variability range are determined by setting $m_{1,2} = -1$ and $m_{1,2} = 1$, respectively, as developed in [25]. On the other hand, if the number of 2D contact elements in the system is more than one, the response boundaries may not be determined manually by assigning some particular values to m; because, in this case, a huge number of combinations with different m values for each fully stuck element can occur. In order to overcome this limitation, we propose an optimization algorithm to determine the response boundaries in every case as

$$\begin{array}{ll} \text{minimize} & \eta \\ \text{with respect to} & [\hat{\mathbf{q}}_s^{\mathrm{T}}, \mathbf{m}^{\mathrm{T}}]^{\mathrm{T}}, \\ \text{subject to} & \mathbf{R} = \mathbf{0} \end{array} \tag{17}$$

where $\mathbf{R}$ is the residual of Eq.(4), and can be defined as

$$\mathbf{R} = \left(-(h\omega)^2 \mathbf{M}_s + ih\omega \mathbf{C}_s + \mathbf{K}_s\right) \hat{\mathbf{q}}_s^h + \hat{\mathbf{F}}_{s,c}^h - \hat{\mathbf{F}}_{s,exc}^h \quad (h = 0, 1, \cdots, H). \tag{18}$$

In Eq. (17), η is calculated as shown in Eq. (10) and it is the objective function to be minimized. Unknown variables of the optimization scheme are the response amplitudes of the fundamental sector, $\hat{\mathbf{q}}_s$, and the vector of multipliers, $\mathbf{m}$. Residual of Eq. (4), $\mathbf{R}$, gets involved into optimization algorithm as the nonlinear constraints to be satisfied. The optimization algorithm given in Eq. (17) looks for the global minimum of the loss factor, which is the case for the lowest damping achieved in the system. Hence, the results of Eq. (17) give the upper boundary of the variability range in response amplitudes. In order to find the lower boundary, the same logic can be used, but with the objective function corresponding to the opposite sign of the loss factor as

$$\begin{aligned} &\text{minimize} && -\eta \\ &\text{with respect to} && [\hat{\mathbf{q}}_s^{\mathrm{T}}, \mathbf{m}^{\mathrm{T}}]^{\mathrm{T}} . \\ &\text{subject to} && \mathbf{R} = \mathbf{0} \end{aligned} \tag{19}$$

Nonlinear dynamic analysis of turbine bladed disks is computationally expensive due to the large number of contact points usually utilized in the models. The computational burden becomes even much higher with an additional optimization scheme since the number of function evaluations severely increases. In order to partly overcome this problem, Craig-Bampton technique [35] to reduce the system matrices and partitioning of the linear and nonlinear DOFs in the solution path [2, 30] are used. There are several optimization strategies in the literature for different purposes. In this study, the interior-point method is utilized. Basically, the interior-point approach approximates the original minimization problem as a sequence of equality constraint problems by adding a barrier function. Interested readers may refer to [36, 37] for a more detailed description of the main theory of the interior-point algorithm. It is not presented here for brevity. Implementation of the optimization process in this study is performed by using *fmincon* built-in function in Matlab. The algorithm uses either a direct step or a conjugate gradient step to solve the approximate problem. The gradients are numerically computed by forward finite difference method. The convergence tolerance in the interior-point algorithm and the error tolerance for the nonlinear constraints are set to 10^{-8}. The whole solution process is briefly summarized in Fig. 6.

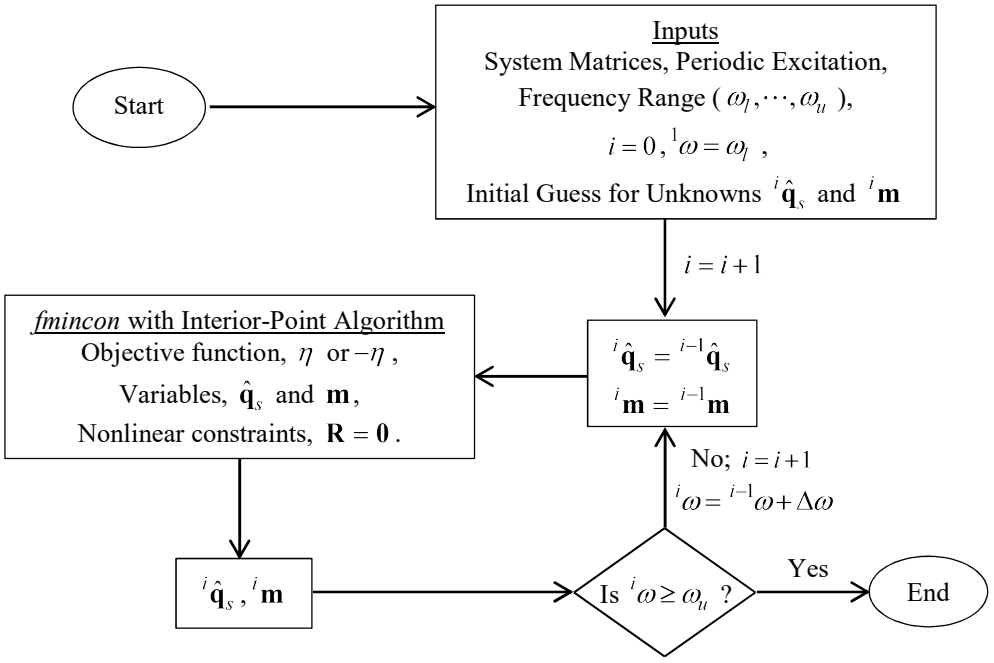

Fig. 6 Flowchart of the Solution Scheme with the Optimization Algorithm

It is worth mentioning that the main aim of this study is to develop a correct framework and to propose a systematic approach that determines the response boundaries with the help of an optimization algorithm. Offering a new numerical optimization method or assessing the most suitable optimization strategy for different problems is out of scope in this study. Here, interior-point algorithm was sufficient for demonstration purposes of the developed methodology with satisfactorily accurate results and a manageable computational cost. However, there may be other optimization methods, which are more appropriate than the interior-point algorithm, for different applications. None of the optimization algorithms can be generalized and would give perfect results for each problem. Nevertheless, it can be said that the global optimization algorithms would be better in capturing the global minima of the objective function with an additional computational cost. This can be seen as a trade-off between robustness and computational burden. Interested readers may also refer to [38] for a basic comparison between several optimization strategies on an engineering design problem.

3. APPLICATION

In this section, the proposed method is validated and demonstrated on the turbine bladed disk depicted in Fig. 1. The model is constructed by using one of the commercial Finite Element programs. The following assumptions are made in the model:

- The bladed disk is considered totally tuned despite the fact that mistuning effects may play an important role on some special turbo-machinery applications.

- Friction contacts are located at the blade shroud and at the blade root.

- The bladed disk considered in this study is constructed for the academic purposes and imitates a realistic geometry of industrial applications.

- The stiffening effect on the bladed disk structure due to rotation is neglected and the system matrices are assumed constant for the response computations within the entire rotational speed interval.

- Micro changes in the contact surfaces are neglected. Contact stiffness of the Jenkins element and friction coefficient of the surface ($\mu = 0.5$) are assumed constant.

- Pre-loads and excitation forces are applied on discrete points.

- Linear damping matrix is created with Classical Rayleigh damping with only stiffness proportion, i.e. $\mathbf{C}_s = 10^{-5}\mathbf{K}_s$.

- The disk is considered rigid and excluded in the analyses. The blade is directly clamped from the root. Gyroscopic effects are neglected.

- In model order reduction with Craig-Bampton approach, reduced system matrices are obtained by retaining the force nodes, response monitoring node and contact nodes as the master nodes, while 50 modal coordinates are taken into account as the slave coordinates.

In order to show the general applicability of the method on different applications, possible source of friction damping at the shrouds and at the blade roots are investigated separately. It should also be noted that the coupled approach with the zeroth and the first harmonics in harmonic balance equations is employed in the solution process. Influence of the higher harmonics on the system response accuracy is out of scope in this work and only the first harmonic is sufficient for the demonstration of the developed method.

3.1 Response Boundaries due to Friction Damping at the Blade Shrouds

The method is firstly applied to the shrouded blades, by assuming no friction damping at the blade roots. Fig. 7a shows the FE model, boundary conditions, excitation nodes and response monitoring node. Since the blade root is clamped, cyclic symmetry only applies through the

shroud contact nodes. Both static pre-load and dynamic excitation are applied from two forcing nodes located at the leading and at the trailing edge of a reference airfoil around 80% of the blade span. Two opposite axial static forces in z and –z directions, respectively, are applied in order to twist the blade and to establish contact at the shrouds during operation. In addition, periodic forces with 100 N amplitudes are applied from the same nodes in all three directions in order to excite multiple blade modes. Response node used to monitor the blade vibration is located in the center of the shroud.

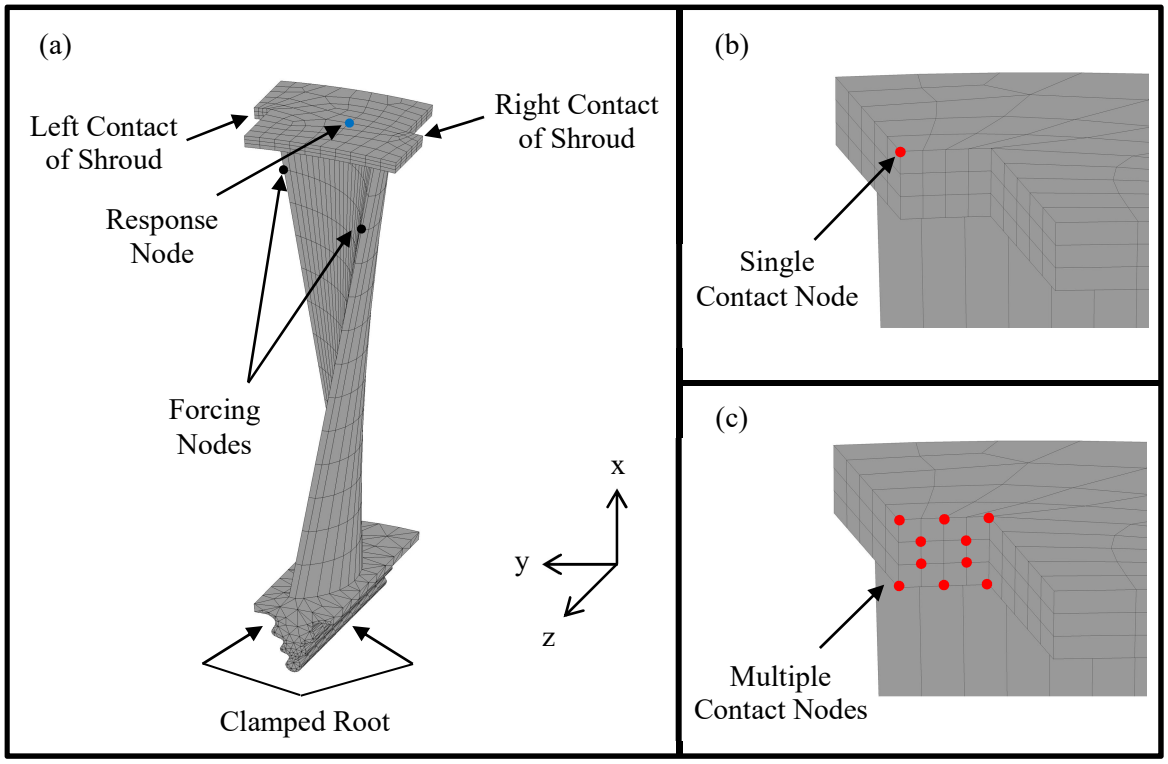

Fig. 7 (a) Finite Element Model, (b) Single Contact Node on Shroud Surface, (c) Multiple Contact Nodes on Shroud Surface

Validation of the method is initially performed on the system with a single contact node as shown in Fig. 7b. This first step allows to prove that the proposed optimization algorithm is theoretically correct, since the developed method can capture the reference boundaries for a simple case whose solution is already available in the literature [25]. Then, the number of contacts is increased and the results for a general case including several contact nodes, as depicted in Fig. 7c, are presented. All the analyses are performed around the first bending resonance region with the 1st harmonic index. The deformed mode shape with the single contact node on the shroud is depicted for the whole turbine bladed disk and the fundamental sector in Fig. 8a and Fig. 8b, respectively. For a better illustration, a color variation is used to depict the mode deflection levels of different regions. Blue and red colors represent the

minimum and maximum deflections, respectively, while the other colors show those in between them. In Fig. 8a, the first nodal diameter among the blades can be clearly seen with the hypothetical blue line in the horizontal middle section of the assembly. In Fig. 8b, the lateral bending mode is highlighted with an interference of the un-deformed (black edge line) and the deformed mode shapes (colored). In case of multiple contact nodes, the mode shape does not change significantly and it is not shown for brevity.

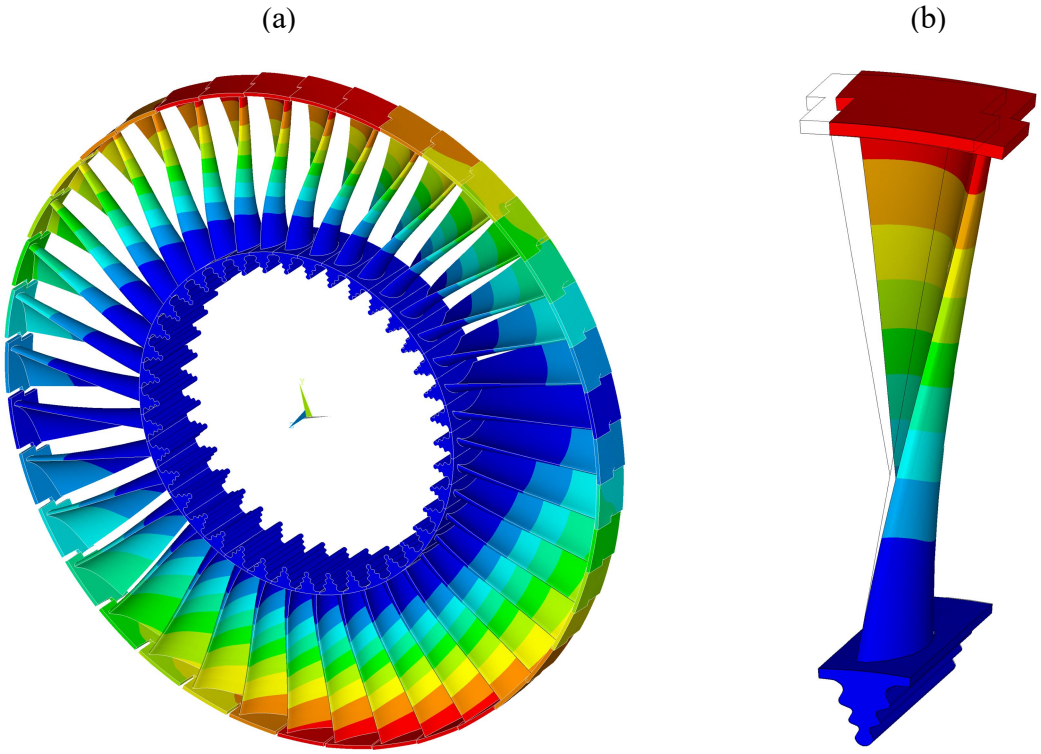

Fig. 8 (a) Investigated Mode Shape of Fully Stuck Linear System for the Turbine Bladed Disk and (b) for the Fundamental Sector

3.1.1 Application with a Single Contact Node

A single contact includes one 2D Jenkins element with two tangential forces in radial and circumferential directions and one normal force in axial direction. Therefore, the contact has a macro-slip motion behavior on the shroud surface in both tangential directions separately. The value of the contact stiffness in tangential and normal directions is assumed same ($k_{t,1} = k_{t,2} = k_n$) and set to 1000 N/μm. It is known from the recent literature [25] that, in the presence of two sliders, when one contact pair is fully stuck, while the other one alternates either stick-slip or stick-slip-separation; multiple solutions exist due to uncertainty of the tangential forces. In these conditions, the response boundaries for macro-slip contact behavior can be determined by using limit tangential forces in the fully stuck element. This strategy developed in [25] is first used here to obtain the reference boundaries. Two nonlinear analyses are performed by

setting $m_{1,2} = 1$ and $m_{1,2} = -1$, respectively, to find the upper and the lower boundaries without utilizing the proposed optimization algorithm.

Fig. 9 shows multiple responses with three different static forces applied on the system. Since the first mode shape of the fully stuck linear system is the lateral bending mode, circumferential displacement amplitudes are shown. Non-unique multiple responses and the variability range corresponding to all three static forces are clearly visible. The reason of this variability is that while the contact is slipping in the circumferential direction, it stays fully stuck in the radial one. Therefore, the uncertainty of the tangential forces in radial static component creates variability in dynamic response calculations. In Fig. 9, the reference boundaries [25], which is obtained manually with limit tangential forces, and those computed with the optimization algorithm are perfectly overlapped, confirming that the choice of the loss factor as the objective function of the optimization algorithm is correct. It should also be noted that, in frictionally damped systems, each contact surface is characterized by a case-dependent threshold F^0_T value, under which 2D gross slip occurs. Hence, the variability range in Fig. 9 shrinks, in agreement with the results presented in [25], as the pre-load F^0 decreases tending towards the shroud threshold value (approximately 2kN in this case).

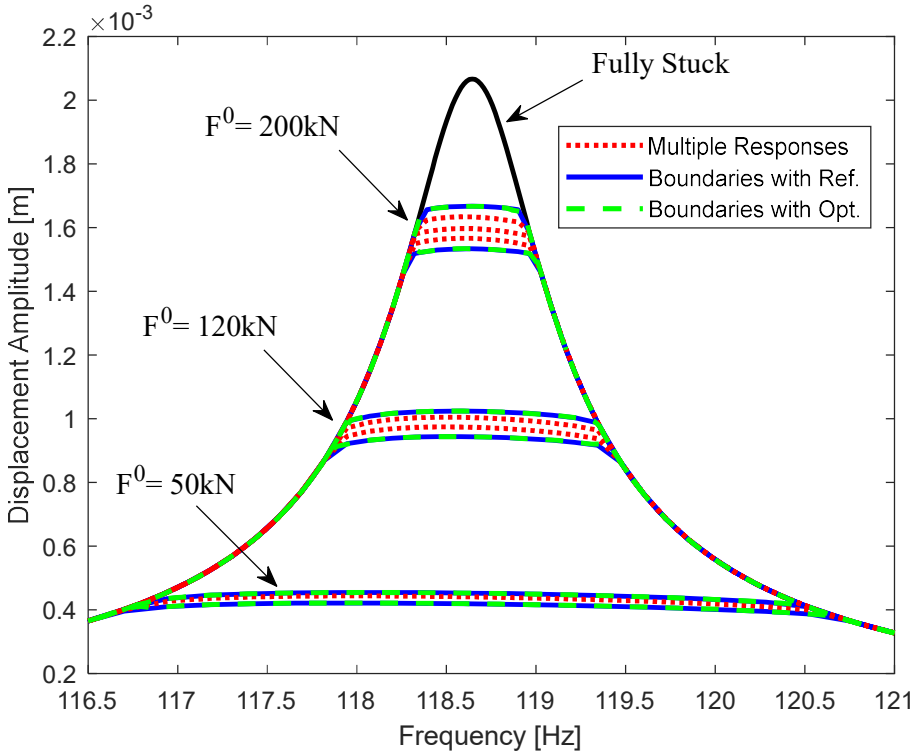

Fig. 9 Multiple Nonlinear Responses with the Boundaries

In the analyses performed with the reference method, m_1 and m_2 are kept constant throughout the entire frequency range and set to –1 and 1; while they vary in the optimization algorithm, since they are additional internal unknowns. For the sake of comparison, the values both m_1 (radial direction) and m_2 (circumferential direction) for the case with $F^0 = 200$kN are shown in Fig. 10a (lower boundary) and in Fig. 10b (upper boundary). Zero initial guess for both multipliers in the optimization is assigned at the very beginning of the analyses and their actual values are obtained at the end of the iterative solution process. The only varying multiplier coefficient in the optimization algorithm is m_1, while m_2 values do not change with respect to initial guess. This indicates that the algorithm searches the global minimum of the loss factor in each analysis by only changing the m_1 value for a certain frequency interval, in which the initial and end points are marked by blue dots and an alternate stick-slip motion occurs in the circumferential direction.

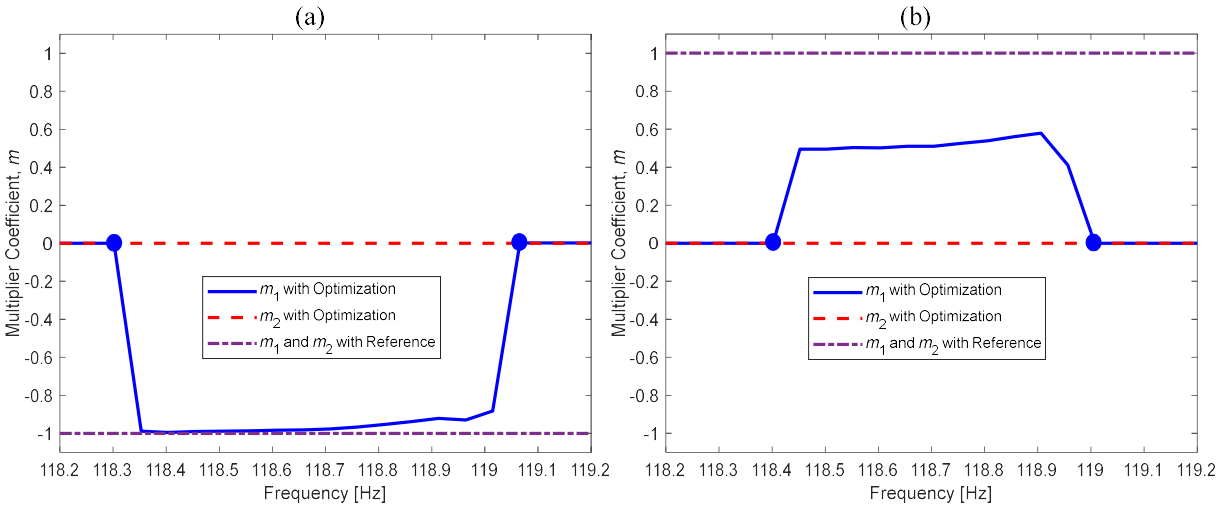

Fig. 10 Values of the Multiplier Coefficients ($F^0 = 200$kN): (a) Lower Boundary Analysis, (b) Upper Boundary Analysis

In Fig. 10, it is also interesting to note that, when alternate stick-slip occurs and the system actually becomes nonlinear, the final value of m_1 computed by the optimization algorithm is different from the reference ($m_1 = \pm 1$). This result confirms that the reference solution strategy proposed in [25] in order to guarantee $T(t_{ini}) = \pm \mu N(t_{ini})$, is conservative with respect to the optimization algorithm. Intermediate guess values ($-1 < m < 1$) could be also enough in some cases to correctly compute the response boundaries. To confirm this observation, the upper response boundary analysis is repeated with the reference method, by setting $m_1 = m_2 = 0.6$. The same results are again obtained, confirming that, in this case, any initial guess with $m_1 \geq 0.6$ and $m_2 \geq 0.6$ allows computing the upper boundary.

3.1.2 Application with Multiple Contact Nodes

Modeling friction interfaces by multiple contact elements introduces more uncertainty, since the number of potential fully stuck contact elements increases. As a result, a huge number of possible combinations is possible with different non-unique static tangential force at each stuck element. Hence, computation of the boundaries with a manual search is totally infeasible and impossible in fact. However, the optimization algorithm proposed in this study overcomes this problem.

Fig. 11 shows the linear responses for free and fully stuck cases and the nonlinear response curves obtained for different pre-loads, F^0. It should be noted that since the turbine bladed disk used in this study is constructed just for academic purposes, the static pre-load applied represents only the twisting effect to retain contact in the shroud interfaces. Contact stiffness for each element in tangential and normal directions is assumed same and arbitrarily assigned to a reasonable value of 100 N/μm.

As can be seen from Fig. 11, there are two response curves given in each case for different pre-loads, although the two curves are either fully or partially overlapped in some cases. These nonlinear responses are computed by the optimization algorithm by minimizing the positive and negative of the loss factor, which results the upper and the lower boundaries, respectively. By doing that, the static and the dynamic balance equations are imposed as the nonlinear constraints. From a general view, the algorithm successfully satisfies these constraints almost in the entire frequency range, while the response jiggles at some particular points. This shows a slight convergence problem took place at some specific frequencies during the iterations, while the general pattern is captured. This can be considered as one of the method's minor drawbacks despite its theoretical correctness. The optimization algorithm, which is implemented by using the *fmincon* function in Matlab, sometimes struggles to satisfy the nonlinear constraints. Nonetheless, the problem here is totally a numerical issue and can be overcome with more correct initial guesses. The authors did not cast a veil over this subject and think that it does not sharply affect the method's great success in capturing the boundaries.

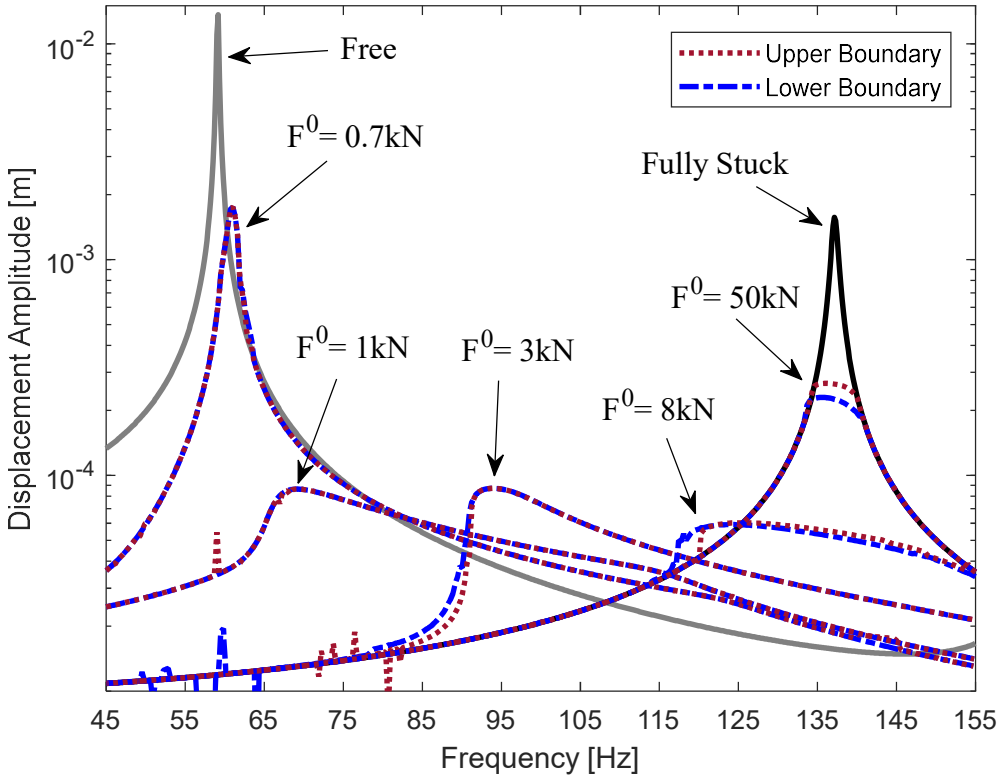

Fig. 11 Frequency Response Curves with the Boundaries

It is clearly seen from Fig. 11 that the variability range throughout the entire frequency range is considerably small. There is even no variability and the response boundaries totally overlap each other for the cases with low-preloads. The deviation slightly increases with higher pre-loads where the difference between amplitudes and resonance frequencies become more apparent. The maximum range in the resonance amplitudes and the resonance frequencies are quite limited around 16% and 1% for the cases with 50kN and 8kN, respectively. This range is considerably smaller than those obtained in presence of either UPDs [23] or mid-span dampers [10]. The main reason for this fact is that UPDs or mid-span dampers used in [23] and [10] have two contact surfaces, where the uncertainty of tangential forces on fully stuck elements at one side strongly affects the other side's normal contact forces. This interaction is defined as the so-called damper-induced cross coupling, since it occurs due to the damper geometry. On the other hand, the frictional interfaces at the shrouds are free from the geometric cross coupling, since both surfaces on the left and right sides have the same contact kinematics and the same periodic contact forces, although shifted in time, due to cyclic symmetry. In this case, the only interaction between tangential and normal contact forces is provided by the dynamic coupling present in the system. Therefore, the effect of uncertainty is smaller, when compared to those of UPDs and mid-span dampers. This observation is also completely coherent with the results presented in [25], where the authors stated that the

variability range is higher with wedge dampers (high cross coupling) with respect to flat dampers (low cross coupling).

A further explanation for the low variability range can also be deduced from the steady-state contact maps depicted for five nonlinear analyses in Fig. 12. Since the main attention is generally focused on maximum amplitudes, contact conditions are presented around the corresponding resonance frequencies. Only one contact map is presented for each range due to the fact that the response variability is considerably small, which enables contact conditions not to differ too much within the range. In Fig. 12a-e, contact nodes at the shrouds are highlighted with respect to their contact conditions. Since, as described in *Section 2.1*, two uncoupled sliders in orthogonal tangential directions have been defined at each contact element, contact status information are provided for both radial (R) and circumferential (C) directions simultaneously. For instance, Fig. 12a illustrates a map at $\omega = 60.9$ Hz for the case with $F^0 = 0.7$kN. It is shown that all the nodes alternate stick-slip-separation in radial direction, while alternating slip-separation occurs in the circumferential direction. As a consequence, unique response exists and there is no variability in the response, as shown in Fig. 11. A similar behavior is also observed at higher pre-loads ($F^0 = 1$ kN and $F^0 = 3$ kN) in Fig. 12b and Fig. 12c, respectively. On the other hand, when the pre-load increases, some contact pairs enter fully-stuck condition during the periodic vibration. For instance, as shown in Fig. 12d for $F^0 = 8$ kN, the whole shroud is in full stick in radial direction, while it is in gross-slip in the circumferential direction. Hence, the uncertainty in the fully stuck contact elements produces non-unique responses. Due to the low coupling between tangential and normal forces, the variability of the response is small. As the pre-load further increases (Fig. 12e, corresponding to $F^0 = 50$kN), the number of fully stuck nodes becomes larger as well as the variability range. The variability vanishes when the shroud is in full stick condition in both directions and a linear behavior is obtained.

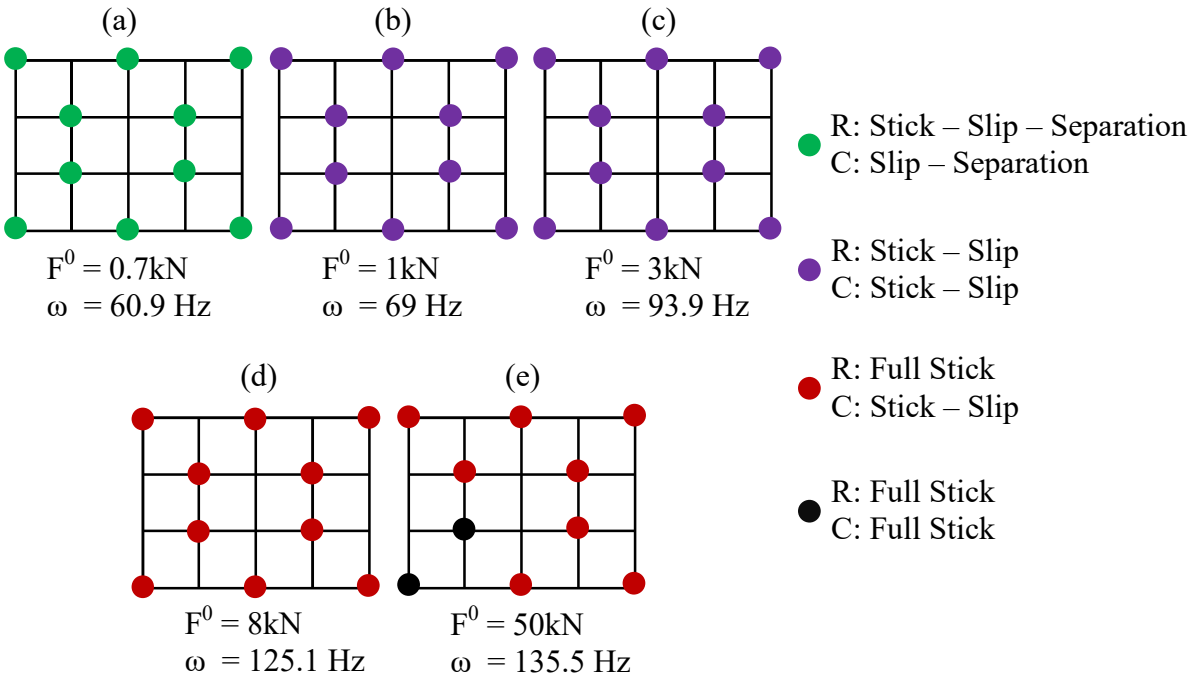

Fig. 12 Contact Conditions on the Frictional Interface of the Shroud

The optimization algorithm proposed in this study overcomes the limitation of a manual search strategy that would imply a large number of simulations without any guarantee of detecting the boundaries. Instead, it represents a systematic approach, based on the minimization of a physical parameter that determines the damping ability of the system. However, the computational effort associated to the optimization algorithm is expected to be higher than the one of a single nonlinear analysis. Table 1 shows a performance comparison in terms of total number of iteration (N_{iter}), total number of function evaluations (N_{eval}) and computational times between the analyses of a manual one (without optimization) and boundaries (with optimization). The values are presented for the overall computation of the analyses characterized by 350 frequency points within a quite wide frequency range (see Fig. 11). All the analyses are performed by a computer with a 4–core processor (Intel(R) Xeon(R) CPU E3–1245 v5 @ 3.50 GHz) and 32 GB RAM. It can be noted that the total number of iterations and function evaluations are higher when the optimization algorithm is used. This also makes the computational cost more expensive. It roughly increases between 2.5 – 7 times for the analyses with different pre-load computations. There is no significant variation between lower and upper boundary analyses since the variability range is small. It should also be noted that *fmincon* function of Matlab is a black-box for the user. It uses either a direct step or a conjugate gradient step to solve the problem. On the other hand, the manual analysis is classically performed by using Newton Raphson with Arc-length Continuation technique. All

the jacobian matrices needed in the iterations for both cases (with and without optimization) are computed numerically with forward finite difference method. It is worth noting that all of the quantitative values shown here is system dependent and they may considerably vary in different systems with a more/less contact elements.

Table 1 Performance Comparison of the Analyses

F^0 [kN]	N_{iter}			N_{eval}			Comp. Time [min]		
	Manual Analysis	Lower Boundary	Upper Boundary	Manual Analysis	Lower Boundary	Upper Boundary	Manual Analysis	Lower Boundary	Upper Boundary
0.7	$1.7x10^3$	$2.7x10^3$	$2.6x10^3$	$3.6x10^5$	$6.1x10^5$	$5.9x10^5$	20	54	52
1	$5.9x10^2$	$2.2x10^3$	$3.5x10^3$	$1.6x10^5$	$5.1x10^5$	$7.8x10^5$	10	46	71
3	$6.3x10^2$	$2.7x10^3$	$2.3x10^3$	$1.7x10^5$	$6.1x10^5$	$5.2x10^5$	10	56	49
8	$1.1x10^3$	$3.5x10^3$	$2.9x10^3$	$2.5x10^5$	$7.6x10^5$	$6.5x10^5$	15	72	62
50	$3.7x10^2$	$1.6x10^3$	$1.9x10^3$	$1.3x10^5$	$3.8x10^5$	$4.4\ x10^5$	8	36	39

3.2 Response Boundaries due to Friction Damping at the Blade Root

In the second case scenario, the blade is assumed to be cantilevered with contact elements (no engaged shrouds), in which the only source of friction damping is at the blade root. Since the disk is modeled as a rigid body, the contact elements ($k_{t,1} = k_{t,2} = k_n = 1000$ N/μm) couple the blade root directly to ground and the blade is a free-free beam without any cyclic symmetry boundary condition applied. Friction surfaces and the location of the contact nodes on each side are shown in Fig. 13. In order to reduce the number of contact nodes and therefore the calculation time, only one lobe of the fir-tree root is used to connect the blade to the ground and 6 contact nodes per side are selected. On both root sides, tangential displacements in u_1 direction are parallel to rotation axis of the bladed disk, while tangential displacements in u_2 acts in the orthogonal direction, being v the normal displacement direction. A radial static force, corresponding to the centrifugal force of the blade, is applied at the forcing and response nodes. In addition, the same periodic excitation provided in the previous case is also applied here.

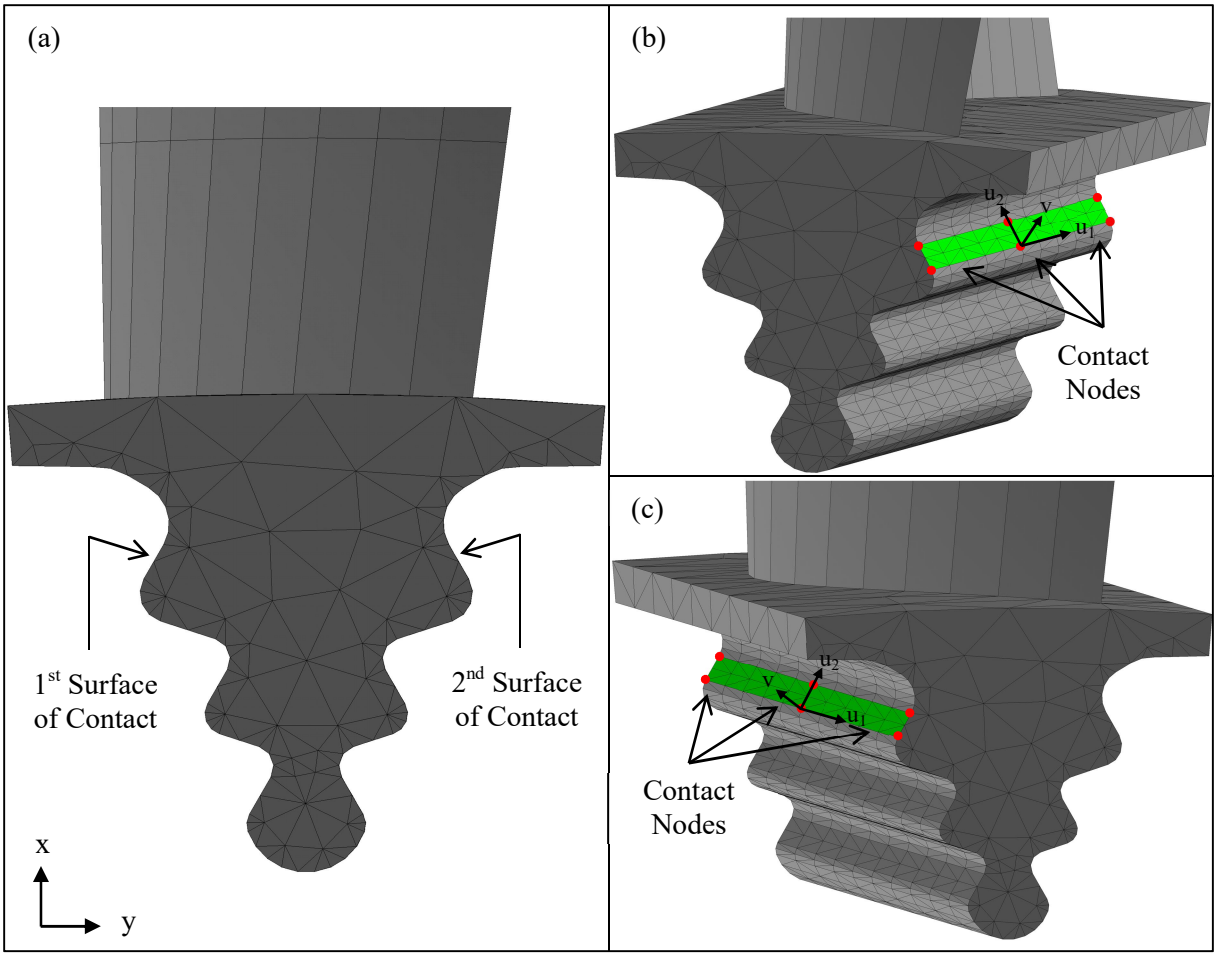

Fig. 13 (a) Contact Surfaces on the Blade Root, (b) Contact Nodes on the 2nd Surface, (c) Contact Nodes on the 1st Surface

The blade's first bending modes in circumferential and axial directions (see Fig. 14) are investigated in order to show the applicability of the method at different resonance regions, characterized by different kinematics at the friction contacts. In order to activate the nonlinearity at the contact, two different values of radial force are applied in the two cases: 500 kN and 30 kN for the first and the second modes, respectively.

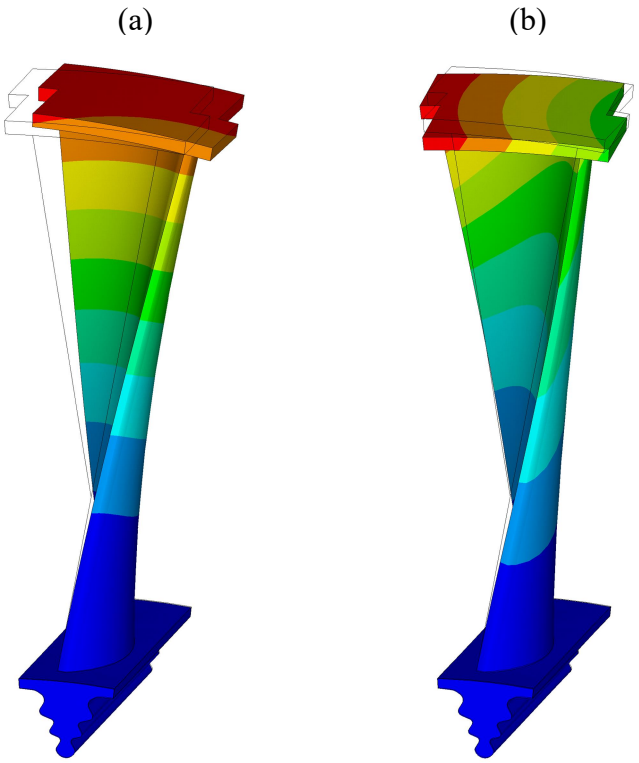

Fig. 14 (a) The 1st Bending (circumferential) Mode Shape, (b) The 2nd Bending (axial) Mode Shape

In Fig. 15a and Fig. 15b, the nonlinear displacement amplitudes of the response node are shown around the first (circumferential) and the second (axial) resonance, respectively. For reference, in both cases, the linear response of the fully stuck blade is also shown. It should be noted that these boundaries represent the theoretical limits that the dynamic response may reach and multiple responses are possible in between them. It is evident that for both resonances, the variability of the response is much larger than the one for the shroud contacts, in terms of vibration amplitudes (8 times for the 1st resonance; 2 times for the 2nd resonance) and frequency shifts (2% and 5%, respectively). There are two main reasons for such a wide variability range. The first one is the geometric coupling between the tangential direction (u_2) of one root side and the normal direction (v) of the other one. This creates more interaction between the contact forces, hence increases the effect of non-unique static tangential forces on the response computation. The second one is the slip behavior at the contact surfaces. In order to explain this further, the contact status at different resonances is investigated in Fig. 16a-d. The left and the right contact surfaces of the root are simply sketched, where the contact nodes are shown and their status is highlighted. A large partial-slip characterizes both contact surfaces at each resonance. In all cases, almost half of the nodes are fully stuck in both local u_1 and u_2 directions. In Fig. 16a-c, the other half mostly alternates stick-slip in u_2 direction

with a full stick motion in u_1 direction. There is full separation at some nodes in Fig. 16d, which implies a loss of stiffness with a considerable resonance shift (see lower boundary in Fig. 15b).

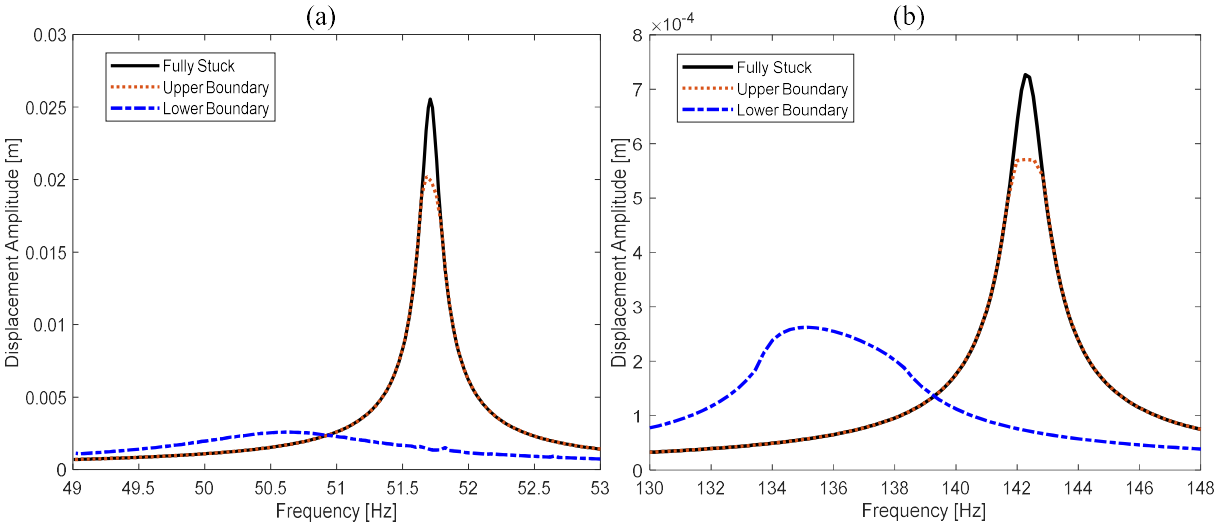

Fig. 15 (a) Responses around the 1st resonance, (b) Responses around the 2nd resonance

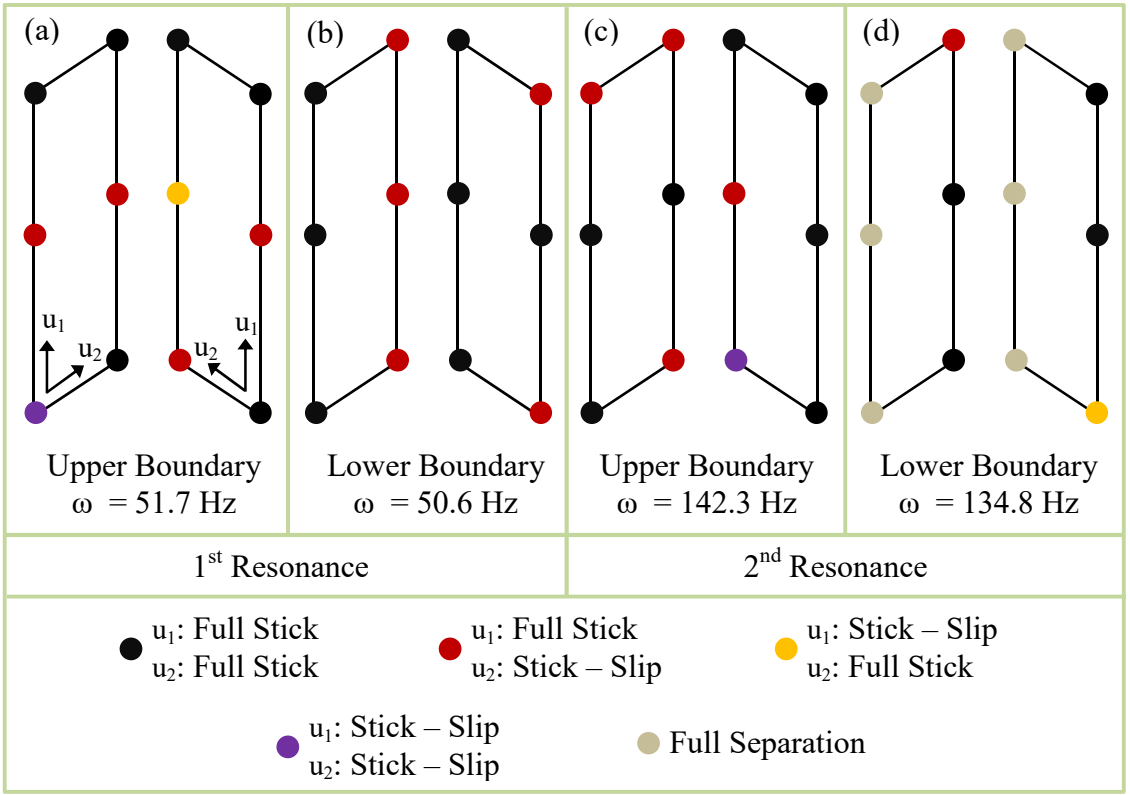

Fig. 16 Contact Conditions on the Friction Interface of the Blade Root

In Fig. 16, it is interesting to note that the number of contact nodes that undergo an alternate stick – slip motion is higher at the upper boundary than at the lower one. This can be puzzling since the amplitudes are much higher in the former configuration. However, it should be

stressed that the amount of time that contacts spend at each contact state considerably differs in the two cases. For instance, considering the map in the upper boundary calculation around the 1st resonance region (Fig. 16a), only one slipping node (at the right side of the root) spends 20% of its periodic vibration cycle in slip state, while it stays 80% in stick state. The rest slipping nodes are actually almost fully stuck (1% and 99% for slip and stick states, respectively). This situation provides a very small amount of damping in the system. On the other hand, in Fig. 16b, all slipping nodes spend approximately 65% and 35% of their cycles in slip and stick states, respectively. Therefore, although the number of slipping node is higher in the former, more damping is provided in the latter.

Another valuable information about the results can be extracted by quantitatively tracking the loss factor computed during the analyses, since it is the ultimate parameter that determines the total damping in the system. Fig. 17a and Fig. 17b illustrate the loss factor, used as the objective function in the optimization process, for the first and the second resonance regions, respectively. The lower boundary is characterized by higher loss factors than the upper one. This result is relevant since the response is more damped in the former, as shown in Fig. 15. In Fig. 17a, the loss factor for both boundaries is almost constant. However, this does not mean that the dissipated energy does not change in the system. Because, the loss factor itself is the ratio between the amount of dissipated energy over the stored one, as defined in Eq. (10). All the curves except the blue one in Fig. 17a also show a bumpy behavior around the corresponding resonance frequencies, which indicates that slip begins and dissipated energy increases in the system. On the other hand, in the frequency interval considered, slip is always present for the lower boundary around the first resonance region. This is why the blue curve of Fig. 17a does not have such kind of behavior, only showing a straight behavior with some jumps at some specific frequencies. It is worth stating here that, although the optimization algorithm successfully satisfies the nonlinear constraints, which means no convergence problem takes place, it finds some local minimum points in these frequencies. Actually, optimization algorithms are generally dependent to initial guess and they may converge to a local minimum point instead of global minimum solutions. The same phenomenon is observed here in this study, as well. Although this effect is not too impactful in this specific case, there may be some other applications where this becomes more relevant. In those situations, one of the easiest remedies may be to change the initial points in order to be in the basin of attraction of the global minimum. This can be achieved by changing the step size and/or the sweep direction of the frequency. Another way is to perturb the objective function

and constraints at various nearby points to check if better results can be obtained than the computed one. Moreover, computing the hessian matrix analytically may also help to obtain correct results, which requires a more sophisticated and further effort in the calculation of gradients. One of the exact solutions is to utilize a global optimization method, where an accompanying drawback of more expensive computational burden is accepted.

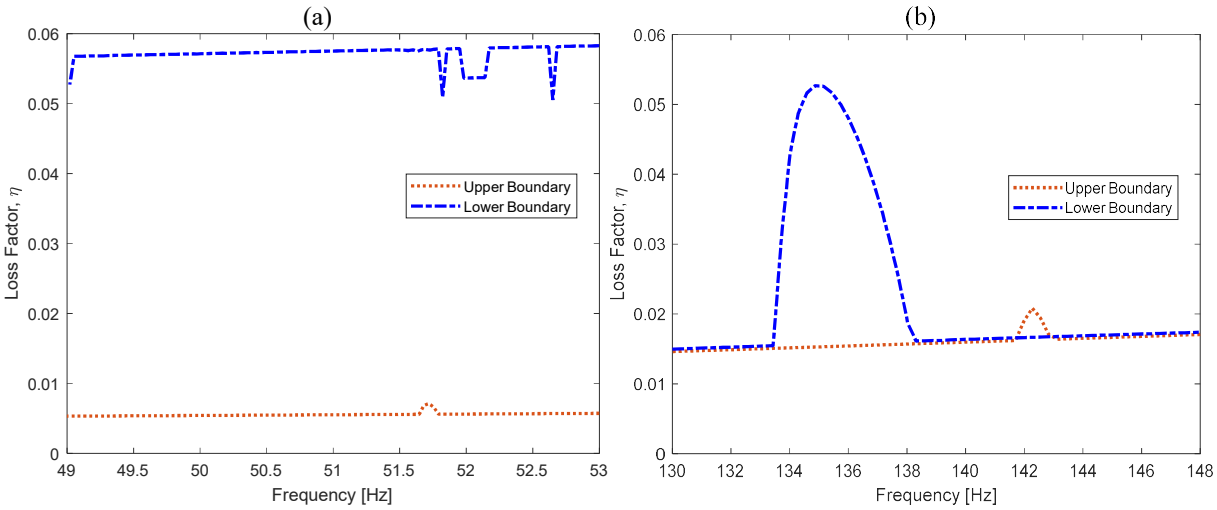

Fig. 17 (a) Change of Loss Factor around the 1st resonance region, (b) Change of Loss Factor around the 2nd resonance region

As in the previous section, performance comparisons are presented in Table 2 for each analysis. Since the frequency interval considered here (see Fig. 15) is narrow compared to shrouded blade case, the number of solution points is smaller (125 and 65 points for the 1st and the 2nd resonance, respectively). The optimization algorithm is considerably more expensive than the single non-linear analysis. This is expected since the number of iteration and function evaluation significantly increases in the optimization. It is also interesting to note that the lower boundary calculation takes more time than the upper one's since the contact in the latter is fully stuck for a larger frequency interval. This provides a unique response in most of the analysis and the algorithm can detect the upper limit faster. On the other hand, in the computation of lower boundary, the partial-slip behavior in the contacts is observed for a wider frequency range. Thus, the optimization algorithm makes a significant number of iterations in the search for the global minimum, which increases the computational burden.

Table 2 Performance Comparison for Different Resonances

	N_{iter}			N_{eval}			Comp. Time [min]		
	Manual Analysis	Lower Boundary	Upper Boundary	Manual Analysis	Lower Boundary	Upper Boundary	Manual Analysis	Lower Boundary	Upper Boundary
1st Res.	$1.9x10^2$	$3.2x10^3$	$5.0x10^2$	$3.2x10^4$	$4.4x10^5$	$8.2x10^4$	1.5	41	7
2nd Res.	$1.1x10^2$	$6.0x10^2$	$3.4x10^2$	$1.8x10^4$	$8.8x10^4$	$5.3x10^4$	1	7.5	5

It is shown in the case studies that the developed method is able to capture the boundaries systematically. However, the response curves computed with the reference method [25] may still attract the reader's attention, in case it will also work for systems with more than two contact elements. The blade root case study suits the best for this purpose, since the variability range is extremely large. Fig. 18 shows the displacement amplitude responses obtained with the reference method, in addition to the ones already given in Fig. 15a. The magenta and the green curves represent the nonlinear response (NLR) obtained by keeping the multiplier coefficient m constant at 1 and -1, respectively, for the entire frequency interval. Hence, the initial guess for the tangential contact force ($T(t_{ini})$) becomes $\mu N(t_{ini})$ and $-\mu N(t_{ini})$ for two different analyses, respectively, as proposed in [25]. As can be seen in Fig. 18, the reference method [25] cannot capture the boundaries, which further highlights the advantage of the developed approach in this paper.

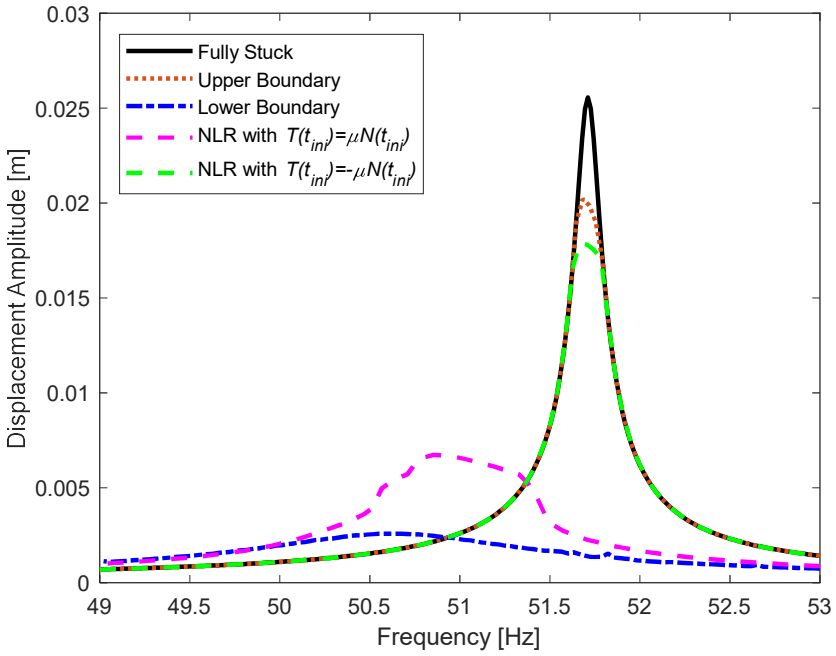

Fig. 18 Response Curves with the Optimization Algorithm and the Reference Method [25]

4. CONCLUSION

Structural dynamics community struggles to reasonably explain the non-repeatable data observed in the experiments of frictional systems. The main reason can be a simple physical fact: the uncertainty phenomenon due to non-unique contact forces. This uncertainty, which has been mostly ignored more than two decades in the literature, may provide a large response variability range, whose boundaries are of the utmost importance from the engineering point of view. In this study, a new numerical approach to determine the response boundaries within the variability range is developed. The method is a generalized technique that utilizes an optimization algorithm to minimize an objective function, being the loss factor of the dynamic system. It is applicable to the different bladed disk configurations, characterized by different friction damping systems, such as blade roots, friction dampers, shrouds, etc. The method is validated and demonstrated on a realistic example by investigating the contact interfaces on the shrouds and on the blade-disk interfaces of an academic bladed disk. The results prove that the method is capable of capturing the periodic response boundaries. In addition to the superior performance of the method, some observations are made throughout the study and they can be summarized as follows;

- Variability range only exists if partial slip is achieved during vibration. In case of fully stuck or gross-slip motion, the uncertainty is lost and a unique response exists.

- Variability range becomes considerably large if the interaction between tangential and normal components is high due to geometric coupling between the contact surfaces that can dissipate energy by friction, as for blade roots and wedge dampers. Therefore, if the main aim is to avoid the uncertainty during operation, non-interacting frictional surfaces that reduce the geometric coupling should be preferred in the design.

- The proposed optimization algorithm successfully determines the response boundaries with an additional computational burden when compared to a single nonlinear analysis. This is quite natural for the optimization processes since the number of function evaluations significantly increases as well as the number of iteration. One possible remedy for this unavoidable consequence is to implement the proposed method into nonlinear modal analysis where the resonance response amplitudes with frequencies can be tracked with the nonlinear mode. This is still an open research area and requires further investigation.

- The aim of the proposed method is to find the global minimum of the loss factor. However, optimization algorithms are generally strongly dependent on the initial guess, which can raise

robustness problem in different analyses. In particular, when the variability range is large, the optimization methods might miss the global minimum and get stuck in one of the local ones. In this study, an interior point algorithm is implemented by using *fmincon* built-in function in Matlab. Although jumps are sometimes observed, it can be generally considered successful as validated in the results section.

- Dynamic algebraic equations, obtained by applying the HBM, are supplied to the algorithm as the nonlinear constraints to be satisfied. However, when the initial conditions are weak, the solution may converge to infeasible points. Since *fmincon* is a black-box to user, an external modification to iteration processes in the nonlinear constraints is limited. It uses either a direct step or a gradient based solution technique. In this study, the hessian and gradient matrices are numerically computed by using forward finite difference method.

To the best of authors' knowledge, the method proposed is the first generalized approach to determine the response boundaries in the context of variability phenomenon. It is applicable and suitable for real life turbine bladed disks with several contacts, although a large number of contact points brings much more complexity and uncertainty to the system with possible negative consequences in terms of convergence. Nonetheless, the authors think that all of these challenges are mainly computational aspects and that the theory of this study represents a very strong framework for the prospective further studies.

APPENDIX

The analytical expressions of the equivalent stiffness and damping terms of a one-dimensional Jenkins element with a constant normal load, N^0, under a single harmonic input motion, i.e. $q(t) = \hat{q}\cos(\omega t)$, are defined as

$$\mathrm{k}_{eq} = \begin{cases} k_t & \text{full stick} \\ \dfrac{k_t}{\pi}\left(\varphi - \dfrac{\sin(2\varphi)}{2}\right) & \text{stick-slip} \end{cases} \quad \text{and} \quad \mathrm{c}_{eq} = \begin{cases} 0 & \text{full stick} \\ \dfrac{4\mu N^0}{\pi\hat{q}}\left(1 - \dfrac{\mu N^0}{k_t\hat{q}}\right) & \text{stick-slip} \end{cases}, \quad (20)$$

where

$$\varphi = \arccos\left(1 - \frac{2\mu N^0}{k_t\hat{q}}\right). \quad (21)$$

REFERENCES

[1] J.H. Griffin, Friction damping of resonant stresses in gas turbine engine airfoils, J. Eng. Power 102(2) (1980) 329-333. https://doi.org/10.1115/1.3230256.

[2] C.H. Menq, J.H. Griffin, A comparison of transient and steady state finite element analyses of the forced response of a frictionally damped beam, J. Vib., Acoust., Stress, and Reliab. 107(1) (1985) 19-25. https://doi.org/10.1115/1.3274709.

[3] C.H. Menq, J.H. Griffin, J. Bielak, The forced response of shrouded fan stages, J. Vib., Acoust., Stress, and Reliab. 108(1) (1986) 50-55. https://doi.org/10.1115/1.3269303.

[4] B.A. Cowles, High cycle fatigue in aircraft gas turbines - an industry prospective, Int. J. Fracture 80(2-3) (1996) 147-163. https://doi.org/10.1007/BF00012667.

[5] K.Y. Sanliturk, D.J. Ewins, A.B. Stanbridge, Underplatform dampers for turbine blades: theoretical modeling, analysis and comparison with experimental data, ASME J. Eng. Gas Turbines Power 123(4) (2001) 919-929. https://doi.org/10.1115/1.1385830.

[6] E. Cigeroglu, N. An, C.H. Menq, Forced response prediction of constrained and unconstrained structures coupled through frictional contacts, ASME J. Eng. Gas Turbines Power 131(2) (2009): 022505. https://doi.org/10.1115/1.2940356.

[7] D. Laxalde, F. Thouverez, J.P. Lombard, Forced response analysis of ıntegrally bladed disks with friction ring dampers, J. Vib. Acoust. 132(1) (2010): 011013. https://doi.org/10.1115/1.4000763.

[8] W. Tang, B.I. Epureanu, Nonlinear dynamics of mistuned bladed disks with ring dampers, Int. J. Nonl. Mech. 97 (2017) 30-40. https://doi.org/10.1016/j.ijnonlinmec.2017.08.001.

[9] J. Szwedowicz, Th. Secall-Wimmel, P. Dünck-Kerst, Damping performance of axial turbine stages with loosely assembled friction bolts: the nonlinear dynamic assessment, ASME J. Eng. Gas Turbines Power 130(3) (2008): 032505. https://doi.org/10.1115/1.2838998.

[10] E. Ferhatoglu, S. Zucca, D. Botto, J. Auciello, L. Arcangeli, Nonlinear vibration analysis of turbine bladed disks with mid-span dampers, Proceedings of the ASME Turbo Expo 2020: Turbomachinery Technical Conference and Exposition. Volume 11: Structures and Dynamics: Structural Mechanics, Vibration, and Damping; Supercritical CO2. Virtual,

Online. September 21–25, 2020. V011T30A020. ASME. https://doi.org/10.1115/GT2020-14942.

[11] E.P. Petrov, D.J. Ewins, Analytical formulation of friction ınterface elements for analysis of nonlinear multi-harmonic vibrations of bladed disks, ASME J. Turbomach. 125(2) (2003) 364-371. https://doi.org/10.1115/1.1539868.

[12] C. Siewert, L. Panning, J. Wallaschek, C. Richter, Multiharmonic forced response analysis of a turbine blading coupled by nonlinear contact forces, J. Eng. Gas Turbines Power 132(8) (2010): 082501. https://doi.org/10.1115/1.4000266.

[13] E.P. Petrov, D.J. Ewins, Effects of damping and varying contact area at blade-disk joints in forced response analysis of bladed disk assemblies, ASME J. Turbomach. 128(2) (2006) 403-410. https://doi.org/10.1115/1.2181998.

[14] D. Charleux, C. Gilbert, F. Thouverez, J. Dupeux, Numerical and experimental study of friction damping blade attachments of rotating bladed disks, Int. J. Rotating Mach. 2006 (2006): 071302. https://doi.org/10.1155/IJRM/2006/71302.

[15] M.R.W. Brake, C.W. Schwingshackl, P. Reuß, Observations of variability and repeatability in jointed structures, Mech. Syst. Signal Process. 129 (2019) 282-307. https://doi.org/10.1016/j.ymssp.2019.04.020.

[16] B.D. Yang, C.H. Menq, Characterization of contact kinematics and application to the design of wedge dampers in turbomachinery blading: part 1—stick-slip contact kinematics, J. Eng. Gas Turbines Power 120(2) (1998) 410-417. https://doi.org/10.1115/1.2818138.

[17] B.D. Yang, C.H. Menq, Characterization of contact kinematics and application to the design of wedge dampers in turbomachinery blading: part 2—prediction of forced response and experimental verification, J. Eng. Gas Turbines Power 120(2) (1998) 418-423. https://doi.org/10.1115/1.2818139.

[18] S. Zucca, D. Botto, M.M. Gola, Range of variability in the dynamics of semi-cylindrical friction dampers for turbine blades, Proceedings of the ASME Turbo Expo 2008: Power for Land, Sea, and Air. Volume 5: Structures and Dynamics, Parts A and B. Berlin, Germany. June 9–13, 2008. pp. 519-529. https://doi.org/10.1115/GT2008-51058.

[19] C.M. Firrone, S. Zucca, M.M. Gola, The effect of underplatform dampers on the forced response of bladed disks by a coupled static/dynamic harmonic balance method, Int. J. Nonl. Mech. 46(2) (2011) 363-375. https://doi.org/10.1016/j.ijnonlinmec.2010.10.001.

[20] S. Zucca, C.M. Firrone, M.M. Gola, Modeling underplatform dampers for turbine blades a refined approach in the frequency domain, J. Vib Control 19(7) (2013) 1087-1102. https://doi.org/10.1177/1077546312440809.

[21] D. Botto, M. Umer, A novel test rig to investigate under-platform damper dynamics, Mech. Syst. Signal Process. 100 (2018) 344-359. https://doi.org/10.1016/j.ymssp.2017.07.046.

[22] D. Botto, C. Gastaldi, M.M. Gola, M. Umer, An experimental ınvestigation of the dynamics of a blade with two under-platform dampers, J. Eng. Gas Turbines Power 140(3) (2018): 032504. https://doi.org/10.1115/1.4037865.

[23] C. Gastaldi, J. Gross, M. Scheel, T.M. Berruti, M. Krack, Modeling complex contact conditions and their effect on blade dynamics, J. Eng. Gas Turbines Power 143(1) (2021): 011007. https://doi.org/10.1115/1.4049186.

[24] M. Stender, M. Jahn, N. Hoffmann, J. Wallaschek, Hyperchaos co-existing with periodic orbits in a frictional oscillator, J Sound Vib. 472 (2020): 115203. https://doi.org/10.1016/j.jsv.2020.115203.

[25] E. Ferhatoglu, S. Zucca, Determination of periodic response limits among multiple solutions for mechanical systems with wedge dampers, J Sound Vib. 494 (2021): 115900. https://doi.org/10.1016/j.jsv.2020.115900.

[26] B.D. Yang, Contact kinematics of friction interfaces and applications to the prediction of resonant response of frictionally constrained turbine blades. PhD Thesis, The Ohio State University, USA, 1996.

[27] T. Butlin, P. Ghaderi, G. Spelman, , W.J.B. Midgley, R. Umehara, A novel method for predicting the response variability of friction-damped gas turbine blades, J Sound Vib. 440 (2019) 372-398. https://doi.org/10.1016/j.jsv.2018.10.013.

[28] T. Butlin, G. Spelman, P. Ghaderi, W.J.B. Midgley, R. Umehara, Predicting response bounds for friction-damped gas turbine blades with uncertain friction coupling, J Sound Vib. 440 (2019) 399-411. https://doi.org/10.1016/j.jsv.2018.08.037.

[29] J. Yuan, A. Fantetti, E. Denimal, S. Bhatnagar, L. Pesaresi, C. Schwingshackl, L. Salles, Propagation of friction parameter uncertainties in the nonlinear dynamic response of turbine blades with underplatform dampers, Mech. Syst. Signal Process. (accepted)

[30] E.P. Petrov, A method for use of cyclic symmetry properties in analysis of nonlinear multiharmonic vibrations of bladed disks, J. Turbomach. 126(1) (2004) 175-183. https://doi.org/10.1115/1.1644558.

[31] T.M. Cameron, J.H. Griffin, An alternating frequency/time domain method for calculating the steady-state response of nonlinear dynamic systems, J. Appl. Mech. 56(1) (1989) 149-154. https://doi.org/10.1115/1.3176036.

[32] O. Tanrikulu, B. Kuran, H.N. Özgüven, M. Imregun, Forced harmonic response analysis of nonlinear structures using describing functions, AIAA J. 31(7) (1993) 1313-1320. https://doi.org/10.2514/3.11769.

[33] C. Siewert, L. Panning, C. Gerber, P.A. Masserey, Numerical and experimental damping prediction of a nonlinearly coupled low pressure steam turbine blading, Proceedings of the ASME Turbo Expo 2008: Power for Land, Sea, and Air. Volume 5: Structures and Dynamics, Parts A and B. Berlin, Germany. June 9–13, 2008. pp. 531-542. https://doi.org/10.1115/GT2008-51073.

[34] J. Chen, C. Zang, B. Zhou, E.P. Petrov, High-fidelity calculation of modal damping caused by friction at blade roots for single blades and tuned bladed disc assemblies, Proceedings of the Institution of Mechanical Engineers, Part C: Journal of Mechanical Engineering Science, June 2020. https://doi.org/10.1177/0954406220935144.

[35] R.R. Craig JR, M.C.C. Bampton, Coupling of substructures for dynamic analyses, AIAA J. 6(7) (1968) 1313-1319. https://doi.org/10.2514/3.4741.

[36] R.H. Byrd, M.E. Hribar, J. Nocedal, An interior point algorithm for large-scale nonlinear programming, SIAM Journal on Optimization 9(4) (1999) 877-900. https://doi.org/10.1137/S1052623497325107.

[37] R.H. Byrd, J.C. Gilbert, J. Nocedal, A trust region method based on interior point techniques for nonlinear programming, Math. Program. 89 (2000) 149-185. https://doi.org/10.1007/PL00011391.

[38] M. Krack, M. Secanell, P. Mertiny, Cost optimization of a hybrid composite flywheel rotor with a split-type hub using combined analytical/numerical models, Struct. Multidiscip. Optim. 44(1) (2011) 57-73. https://doi.org/10.1007/s00158-010-0573-z.